PERGAMON

GEOTHERMICS

Geothermics 31 (2002) 303–342

www.elsevier.com/locate/geothermics

Monitoring production using surface deformation: the Hijiori test site and the Okuaizu geothermal field, Japan

Don W. Vasco[a,*], Kenzi Karasaki[a], Osamu Nakagome[b]

[a]*Division of Earth Sciences, Building 90, Lawrence Berkeley National Laboratory, Berkeley, CA 94720, USA*
[b]*Japan Petroleum Exploration Co. Ltd., 2-2-2 Higashishinagawa, Shinagawaku, Tokyo 140-0002, Japan*

Received 5 March 2001; accepted 5 October 2001

Abstract

Production in geothermal reservoirs often leads to observable surface displacement. As shown in this paper, there is a direct relationship between such displacement and reservoir dynamics. This relationship is exploited in order to image fluid flow at two geothermal field sites. At the first locality, the Hijiori Hot Dry Rock (HDR) test site, 17 tilt meters record deformation associated with a 2.2 km deep injection experiment. Images of fluid migration along a ring fracture system of the collapsed Hijiori caldera are obtained. At the Okuaizu geothermal field, leveling and tilt meter data provide constraints on long- and short-term fluid movement within the reservoir. A set of 119 leveling data suggest that the north-to-northeast trending Takiyagawa fault acts as a barrier to flow. The northwesterly oriented Chinoikezawa and Sarukurazawa faults appear to channel fluid from the southeast. The tilt data from Okuaizu indicate that a fault paralleling the Takiyagawa fault zone acts as a conduit to transient flow, on a time scale of several weeks. The volume strain in a region adjacent to the injection wells reaches a maximum and then decreases with time. The transient propagation of fluid along the fault may be due to pressure build-up, resulting from the re-initiation of injection. Published by Elsevier Science Ltd on behalf of CNR.

Keywords: Subsidence; Surface tilt; Inverse problems; Hijiori; Okuaizu; Japan

* Corresponding author. Tel.: +1-510-486-5206; fax: +1-510-486-5686.
E-mail address: dwvasco@lbl.gov (D.W. Vasco).

0375-6505/02/$22.00 Published by Elsevier Science Ltd on behalf of CNR.
PII: S0375-6505(01)00036-0

1. Introduction

When fluid is extracted from or injected into a reservoir the stress field in the surrounding rock is changed, inducing strain. The subsurface strain propagates upward, ultimately deforming the Earth's surface (Hatton, 1970; Narasimhan and Goyal, 1984). Often this associated deformation is viewed as an undesirable feature of geothermal production. In some cases, such as the Wairakei field in New Zealand, the displacements are large enough to induce structural damage (Allis, 2000). However, surface deformation can provide useful information, related to the mass, pressure, and temperature changes within a geothermal reservoir. In particular, surface deformation data may be used to image reservoir dynamics, the response of a reservoir to production. For example, surface displacements may be used to infer the location and orientation of a fracture or fault zones. Fluid and heat flow in many geothermal fields is controlled by the presence and geometry of such faults and fractures. In contrast to layers with well-defined boundaries, it can be extremely difficult to locate and characterize the distribution of fractures in the subsurface. More problematic is the determination of those faults and fracture zones which are conductive pathways for fluids. Even if the geometry of a conductive fracture zone or fault zone is known, there are typically significant variations in permeability within the zone itself. Wells may penetrate a fault zone and still be non-productive.

The motion of the Earth's surface has been used to image fault rupture (Langbein, 1981; Ward and Barrientos, 1986; Segall and Harris, 1987). Observations of surface displacement have also been used to infer fluid movement associated with magmatic systems (Mogi, 1958; Savage and Clark, 1982; Vasco et al., 1988, 1990; Wicks et al., 1998). Both leveling and tilt data have been used to monitor shallow injections (Du et al., 1993; Vasco et al., 1998), hydrofracturing (Evans et al., 1982; Palmer, 1990; Castillo et al., 1997; Wright et al., 1998), fluid migration within petroleum reservoirs (Dussealt et al., 1993; Bruno and Bilak, 1994; Fielding et al., 1998; Vasco et al., 2000; Stancliffe and van der Kooij, 2001), aquifer compaction (Galloway et al., 1998; Hoffman et al., 2001) as well as geothermal production (Lofgren, 1978; Denlinger et al., 1981; Mossop and Segall, 1999). One useful feature of geodetic data is that it is measured at the Earth's surface or in shallow boreholes. Thus, geodetic observations are typically much less expensive than are measurements requiring deep boreholes, such as transient pressure data. New technologies, such as interferometric synthetic aperture radar (InSAR), can provide relatively inexpensive, high resolution images of surface deformation. This methodology is proving useful in mapping subsidence related to geothermal production (Vadon and Sigmundsson, 1997; Massonnet et al., 1997; Carnec and Fabriol, 1999; Fialko and Simons, 2000; Vasco et al., 2001a).

The utility of geodetic data in constraining the dynamics of geothermal systems is highlighted in this paper. The methods are illustrated with three sets of observations from geothermal sites in Japan. The first is a collection of tilt meter observations associated with pumping tests conducted at the Hijiori test site. The second set of data consists of leveling measurements obtained at the Okuaizu geothermal field. The leveling data record vertical deformation due to field operations from 1997 to

1998. The third set comprises tilt data, again from the Okuaizu geothermal field. These data are used to image the transient response of the reservoir to the initiation of injection and production, following a field-wide maintenance program in the summer of 2000.

2. Methodology

Here we outline the inverse problem of estimating reservoir volume changes, given a set of geodetic observations. That is, based upon a set of measurements, such as leveling, tilt, or three-dimensional displacements, we wish to infer the distribution of volume change within the reservoir which could produce such deformation. The treatment will be brief, as more in-depth descriptions of the approach can be found elsewhere (Vasco et al., 1988, 1998, 2000). As is typical of inverse problems, there is the issue of non-uniqueness: many distributions of volume change may produce the same surface deformation at the observation points. One way to attack this issue is the construction of the model parameter resolution matrix, a quantitative measure of non-uniqueness (Menke, 1989; Parker, 1994). See Vasco et al. (2001a) for a discussion of this issue in a context very similar to ours: estimating subsurface volume change from surface displacement data.

2.1. Relating surface deformation to reservoir volume change

Production or injection associated with the operation of a geothermal field results in mass flux within the reservoir. In response to this flux the reservoir typically deforms, undergoing a volume change. Note that the volume change may be induced by either a change in pressure or temperature; we shall not make a distinction. The measure of volume change considered here is the stress free volume strain, $\Psi(x)$ (Vasco et al., 1988). The stress-free volume change is given by

$$\Psi(\boldsymbol{x}) = \Delta e_{11} + \Delta e_{22} + \Delta_{33}$$

where Δe_{ll} are stress-free strain components (Aki and Richards, 1980, p. 60). The relationship between the stress-free or transformational strain, which is the strain that a volume would undergo in the absence of a surrounding elastic matrix, and the constrained strain (strain in the presence of the matrix) is described in Eshelby (1957).

As shown in Vasco et al. (1988), one may represent the n-th component of surface displacement at x by an integration over all volume strain within the reservoir

$$u_n(x) = \int_V g_n(x, y)\Psi(y)\mathrm{d}y \tag{1}$$

where $\mathrm{g_n}(x, y)$ is the Green's function, the response at x due to a point-volume change at y and V denotes the reservoir volume. Thus, the n-th component of displacement at point x is an integral of the transformational volume strain within the

reservoir. In the inverse problem one solves Eq. (1) for the distribution $\Psi(y)$, given a discrete set of displacement observations, $u_n(x_i)$. In the current applications, we implement an analytical Green's function $g_n(x, y)$ for a uniform half-space. The solution is based upon a generalization of the results of Maruyama (1964), as described by Vasco et al. (1988). The modified Green's function is expressed as

$$g_n(x, y) = \frac{(\nu + 1)}{3\pi} \frac{(x_n - y_n)}{S^3} \tag{2}$$

where ν is Poisson's ratio and

$$S = \sqrt{(x_1 - y_1)^2 + (x_2 - y_2)^2 + (x_3 - y_3)^2} \tag{3}$$

is the distance from the source point to the observation point. For a more complicated model of the medium one can resort to purely numerical methods to compute the integral of the point response over a cell volume, as described in Vasco et al. (2000).

2.2. Discretization and model parameter estimation

In formulating the inverse problem, it is necessary to discretize the reservoir volume change distribution. Essentially, the reservoir volume is subdivided into a large number of cells or blocks, each of which may undergo a volumetric expansion or contraction. The contribution of a particular cell, say block j, to the n-th component of displacement at the surface is given by

$$u_n^j(x) = \psi_j \int_{V_j} g_n(x, y) \mathrm{d}y \tag{4}$$

where V_j denotes the region occupied by cell j, and ψ_j denotes the stress-free fractional volume change in the cell. The total fractional volume change in the reservoir is a summation over all component cells. Hence, for M cells, the accumulated displacement at x_i is given by

$$u_n(x_i) = \sum_j^M u_n^j(x_i) = \sum_j^M G_{ij}^n \psi_j \tag{5}$$

where

$$G_{ij}^n = \int_{V_j} g_n(x_i, y) \mathrm{d}y \tag{6}$$

Given a large number of observations (say N), at various points on the Earth's surface, constraints of the form (5) comprise a linear system of equations. The linear system of equations may be written in vector-matrix notation as

$$\mathbf{u} = \mathbf{G}\boldsymbol{\Psi} \tag{7}$$

We can solve Eq. (7) for the fractional volume changes in the cells $\boldsymbol{\Psi}$. As noted in Vasco et al. (1998), in order to stabilize the inverse problem, one augments the linear data constraints by regularization constraints (Menke, 1989). In essence, regularization constraints are penalty terms that are minimized in conjunction with the minimization of the misfit to the data. The penalty terms are measures of model properties such as the size of the model perturbations or the roughness of the model (Menke, 1989; Parker, 1994). The application of these techniques to the estimation of volume change is described in Vasco et al. (1998, 2000). The regularized linear equations are solved by any standard linear system solver (Golub and Van Loan, 1989).

2.3. Model assessment and resolution

For a fine discretization of the subsurface, large M in Eq. (5), volume change estimates for individual cells cannot be uniquely determined. Rather, only spatial averages of the properties of interest can be estimated reliably. Consideration of the scale at which variations in fractional volume change may be reliably estimated leads to the idea of model parameter resolution and the resolution matrix (Menke, 1989).

The functional form of the resolution matrix follows from the assumption that there is a 'true' model, $\boldsymbol{\Psi}_t$, related to the data by Eq. (7). However, because the system of Eq. (7) is ill-conditioned when M is large, it cannot be solved directly. Rather, an estimate of the model parameters is the result of inverting or solving Eq. (7) along with the regularization needed to render the inversion stable (Menke, 1989; Parker, 1994). Because the inverse problem is linear, model parameter estimates $\hat{\boldsymbol{\Psi}}$ are linearly related to the observations

$$\hat{\boldsymbol{\Psi}} = \mathbf{G}^{\dagger}\boldsymbol{u} \tag{8}$$

where $\mathbf{G}^{\dagger}$ denotes the generalized inverse that incorporates the regularization in solving Eq. (7). Substituting the expression (7) for $\mathbf{u}$ into Eq. (8), noting that $\boldsymbol{\Psi}$ is our 'true' model $\boldsymbol{\Psi}_t$, one arrives at

$$\hat{\boldsymbol{\Psi}} = \mathbf{G}^{\dagger}\mathbf{G}\boldsymbol{\Psi}_t \tag{9}$$

or

$$\hat{\boldsymbol{\Psi}} = \mathbf{R}\boldsymbol{\Psi}_t \tag{10}$$

where $\mathbf{R}$ is the resolution matrix relating our estimates to the hypothetical 'true' model.

The resolution matrix may be interpreted as a linear filter through which the actual spatial distribution of flow properties is viewed. The rows of the resolution matrix are averaging coefficients indicating the contribution of all other parameters to an estimate for a given cell. In the ideal case the resolution matrix would be an identity matrix and the properties of each cell are perfectly resolved. In such a case

there is no trade-off with estimates for adjacent cells. One advantage of the resolution matrix is that it is independent of the data uncertainty and only depends on our sensitivities and the geometry of our experiment.

3. Applications

3.1. Pump test at the Hijiori test site

3.1.1. Geologic setting

Hijiori is a collapsed caldera approximately 1.5–2 km in diameter. The Holocene Hijiori volcano, which erupted about 10,000 years ago, is situated above a Cretaceous granodiorite basement (Kitani et al., 1998). The top of the granodiorite dips slightly to the north and east and varies in depth from about 1500 to 2000 m. The granodiorite is altered by at least three phases of hydrothermal metamorphism. Overlying the caldera basement are rock units of varying thickness (Kitani et al., 1998). The structure at Hijiori is dominated by the collapse of the volcano and caldera formation. In particular, an extensive system of ring fractures and faults has developed, bounding the caldera center (Fig. 1). The faults are all steeply dipping, with most dips greater than 70 ° (Kitani et al., 1998). The main concentration of hot springs and fumaroles is found at the eastern edge of the caldera, along a north to northeast trending fault. There is a gravity low associated with the southern portion of the Hijiori caldera which is thought to be due to hydrothermal alteration in the subsurface (Kitani et al., 1998).

The Hijiori test site consists of a total of 12 wells drilled into the Holocene volcanic caldera (Kitani et al., 1998). Many of the initial wells were exploratory, in the hope of finding a convective geothermal system for power generation. Since 1985 the site has been operated by the New Energy and Industrial Technology Development Organization (NEDO) of Japan as a test site for hot dry rock (HDR) development techniques. Four primary wells, situated at the southern edge of the caldera, comprise the Hijiori test site proper. During the 1990s several circulation tests were performed at the test site. The first, in 1991, was conducted in what is termed the shallow reservoir (1600–1900 m). The length of the test, 90 days, was sufficient to obtain cool-down curves for multiple production horizons in the reservoir (Kruger and Yamaguchi, 1993). Following this test a well, HDR-1 (Fig. 1), was extended to over 2200 m and hydraulically stimulated to create what is referred to as the deep reservoir. Well HDR-1 was cased down to 2151 m in order to prevent a direct connection to the upper reservoir. One-month circulation tests were then conducted in 1995 and 1996. A longer term circulation test, of 2 years duration, is now underway and should continue until 2002 (Kuriyagawa and Tenma, 1999).

The conceptional model developed for the Hijiori test site consists of two major fractures or faults, intersecting the reservoir wells at about 1800 and 2200 m (Swenson et al., 1999). In general, there is less connectivity in the deeper fracture system than in the shallow reservoir (Tenma et al., 1997). The features are part of the ring fracture-fault system encircling the caldera (Fig. 1). The two ring fractures

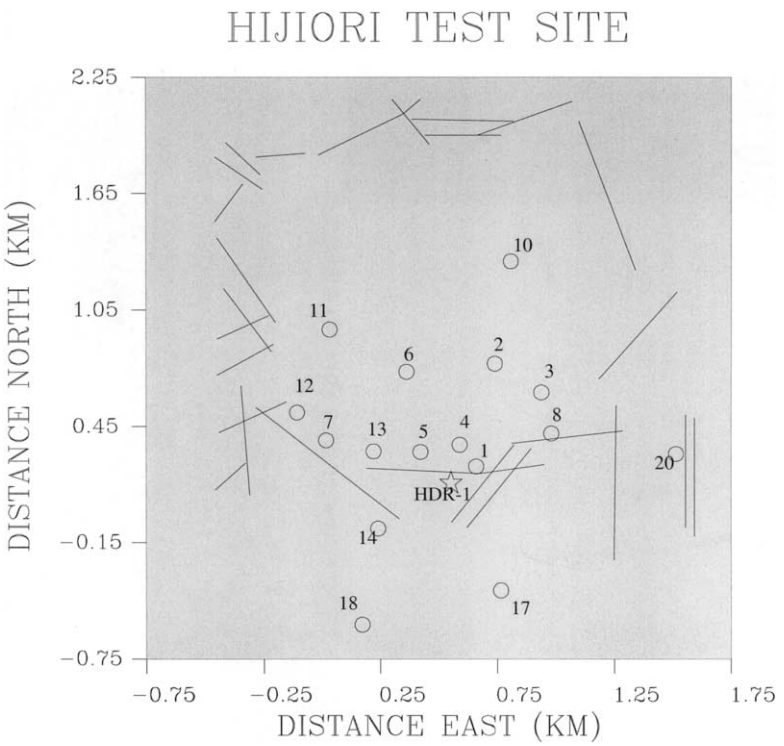

Fig. 1. Experimental layout for the Hijiori tiltmeter experiment. The tiltmeter locations are indicated by open circles and the instrument number. The line segments indicate surface locations of mapped faults (after Kitani et al., 1998). The bottomhole location of the pumping well HDR-1 is indicated by a star.

strike approximately east-west and dip steeply, about 70°, to the north (Swenson et al., 1999). The fractures and faults are thought have a higher fluid conductivity overall, though the permeability is quite variable within the zones themselves. Note that this model is to some degree a simplification of the subsurface conditions at Hijiori. For example, there is a large number of fractures intersecting the wells, with fracture densities of up to 24 fractures per meter (Kitani et al., 1998). Some nine to ten effective fractures have been identified in surrounding wells from pressure-temperature spinner logs. The fractures strike approximately east-west (76–94° east of north, dipping 73°), forming a system of roughly parallel fracture planes. Furthermore, there is evidence of communication between the upper and lower reservoirs, indicating conductive fracture intersections. A major uncertainty in interpreting the Hijiori circulation tests has been the flow paths within the reservoir. For example, in circulation tests within the deeper reservoir only about 40% of injected fluid is recovered by producing wells that are only 90 and 130 m away. General indications from acoustic emission data and circulation test data are that a significant portion of the fluid loss is to the east of the injector HDR-1 (Kuriyagawa and Tenma, 1999).

3.1.2. Tilt monitoring of pumping tests

In order to test the capability of tilt meters for mapping fluid flow, a series of injection tests were conducted in the deeper fracture zone in the fall of 1999. In these tests a total of 20 tilt meters were installed in boreholes, within and around the Hijiori caldera (Fig. 1). The instruments are high precision (one nanoradian) instruments with an internal leveling device (Castillo et al., 1997; Wright et al., 1998). The tilt meters were emplaced in shallow boreholes, approximately 12 m deep, in order to shield them from near-surface temperature variations. The pumping well was HDR-1, and the injection interval was from a depth of 2151 m (the bottom of the casing) to 2205 m (the bottom of the well). The open interval is about 500 m below the floor of the caldera (Kitani et al., 1998). These tests followed a similar experiment conducted in 1998 (Vasco et al., 2000).

The injection tests were conducted with two purposes in mind: testing a newly developed system for sinusoidal injection and reservoir monitoring using tilt meters. Because of these dual objectives, the injection history was not optimal for isolating the tilt signal due to particular injection events. This is apparent from an examination of the injection rate histories for six days, just prior and during the two tests [Fig. 2(a) and (b)]. An ideal situation would be initially quiet conditions (no pumping) followed by sudden injection at a fairly constant high rate. However, prior to our first test, at about 8.54 days, there was significant flow into the reservoir associated with the testing of the sinusoidal injection system. Similarly, for at least four days prior to the tilt meter experiments (days 4–7), there was notable injection to test the pumping system. This pre-test injection has the effect of pressurizing and cooling the reservoir in a complex fashion (Nakagome et al., 1994). Also, it complicates the pre-experiment tilt signal, making it more difficult to remove the background drift from each tilt series.

The raw tilt observations were scaled and rotated into a geographic coordinate system in which positive X corresponds to tilt to the east and positive Y corresponds to tilt to the north. Also, static shifts and linear drifts, for the time interval 5.5–8.0 days, were removed from the observations. Three of the borehole tilt meters (9, 15 and 19) did not provide useful signals and are not included in our analysis. For many instruments there was significant variation prior to days 8 and 9, the days of the experiments (Fig. 3). Much of the variation is due to Earth tides, a periodic signal due to the gravitational pull of the sun and moon. For most tilt meters the magnitude of the Earth tides is 0.1–0.2 μrad. On some instruments, most notably tilt meter 1, there are large variations (up to 1 μrad in magnitude) prior to our injection tests. These variations are likely due to the testing of the sinusoidal injection system. At the scale of the plots it is difficult to discern any direct correlation with the injections on days 8 and 9 [Fig. 2(b)]. What is remarkable is the dramatic long period tilt that commenced near the beginning of the two experiments and continued beyond the conclusion of final injection (Fig. 3). This variation is not in direct correspondence with the stop and start of any one particular injection episode. In fact, the largest change in surface tilt occurred during the night, between the injection events. The observed tilt variation is very large in comparison to all pre-injection variations. Furthermore, the long period changes are unambiguous on nine

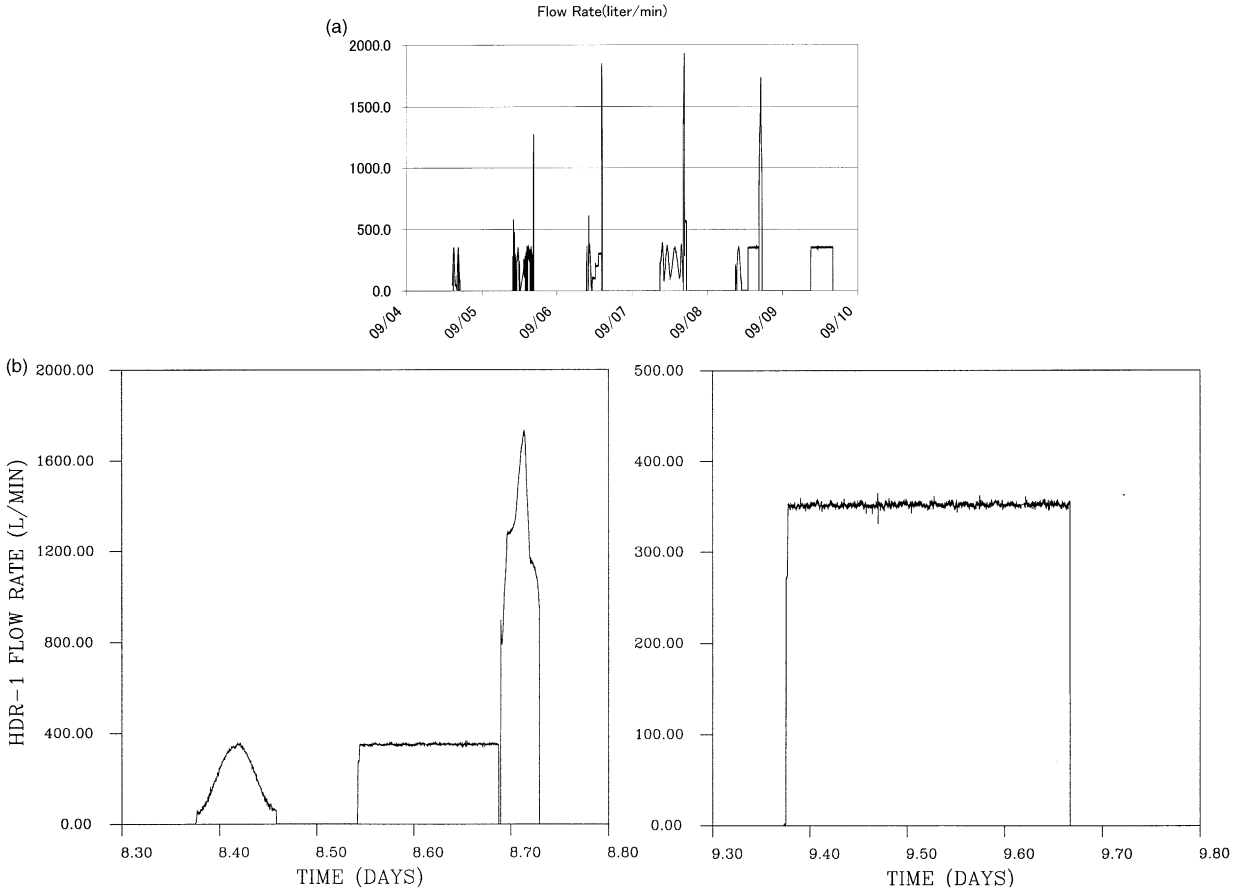

Fig. 2. (a) Flow rates for six days encompassing the tilt meter injection tests. The variations in flow rate associated with the testing of the sinusoidal pumping system are evident. (b) Flow rates associated with the two injection experiments (days 8 and 9).

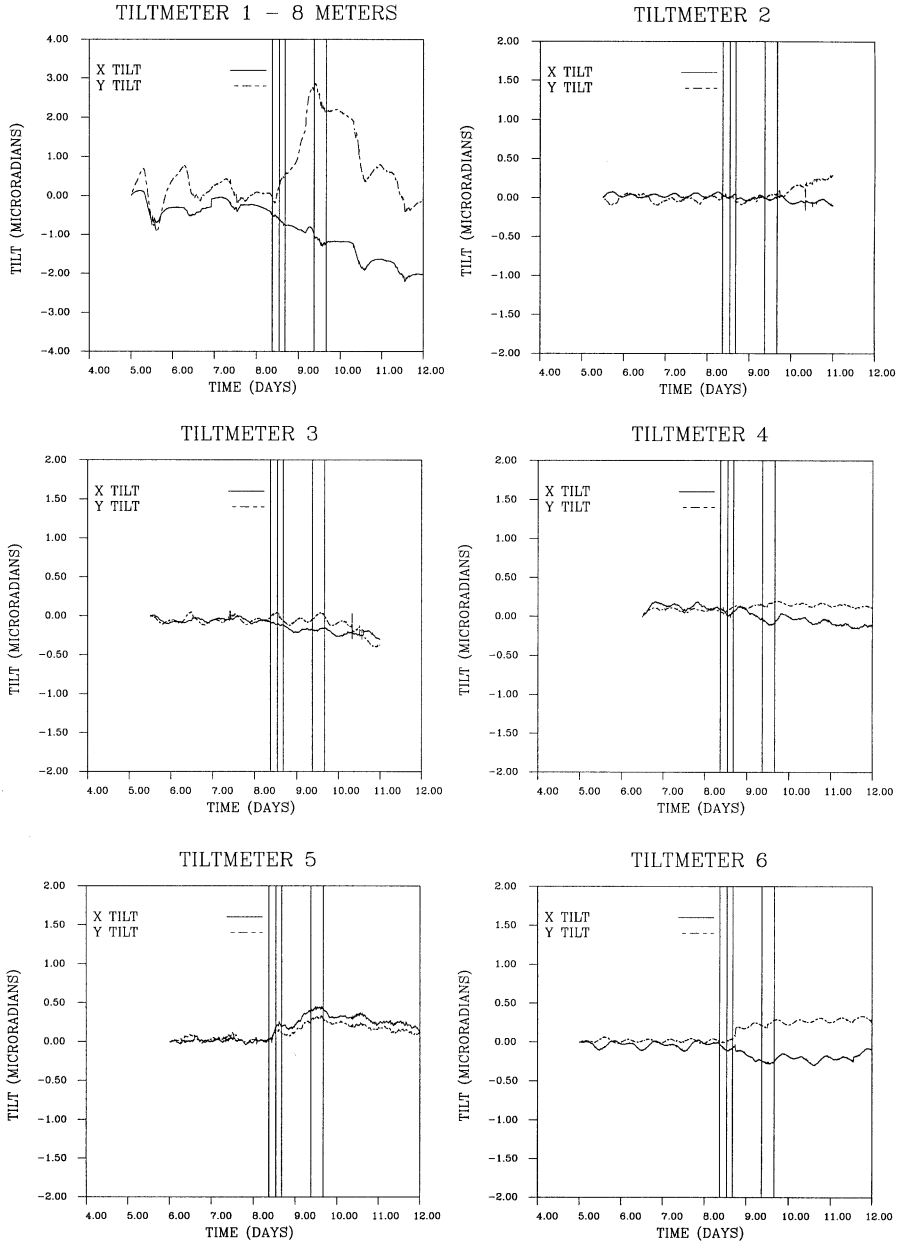

Fig. 3. X and Y components of surface tilt for days 5–12. The first vertical line indicates the initial injection on day 8, the sinusoidal flow rate in Fig. 2(b). The next four vertical lines represent the stop and start times of the two constant-rate injection tests that followed [Fig. 2(b)].

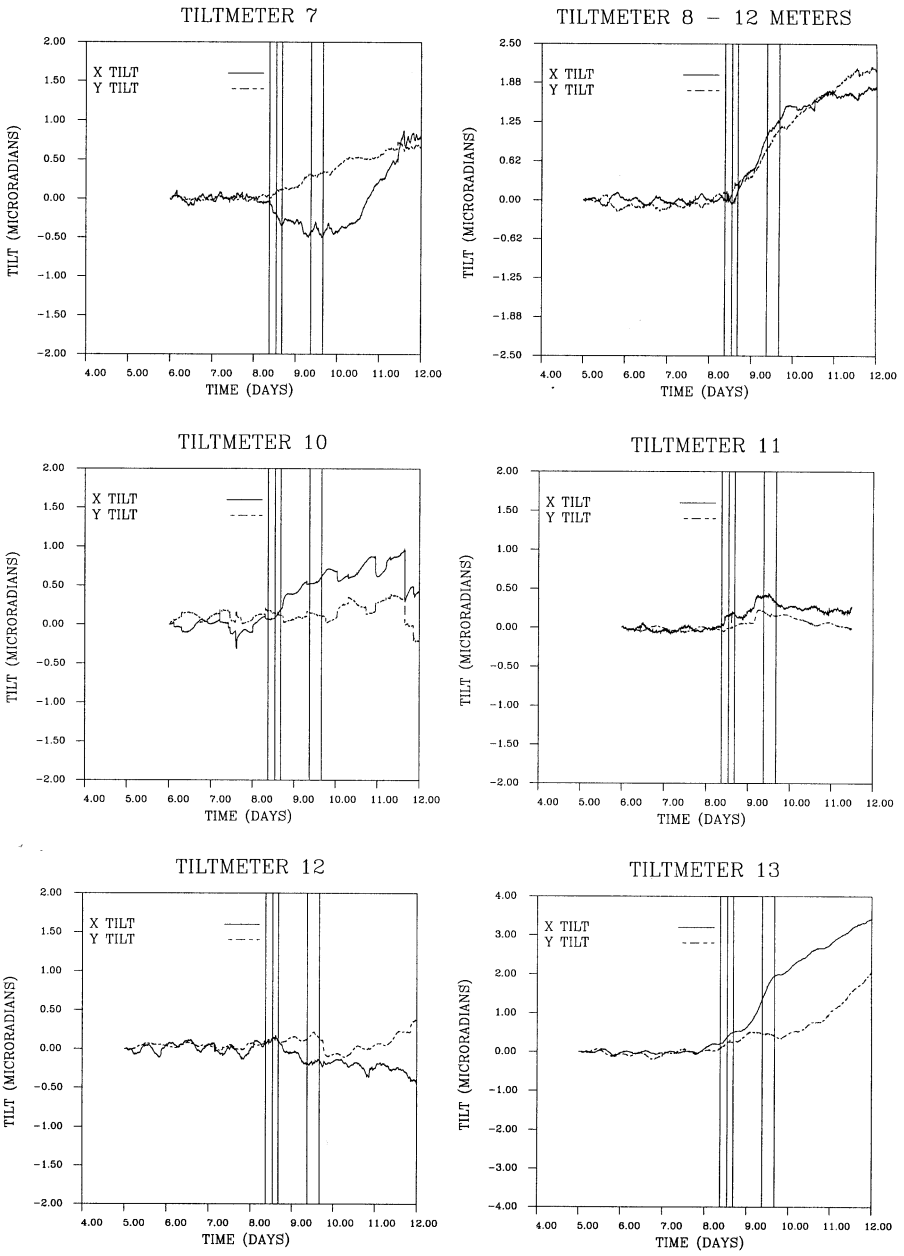

Fig. 3 (*continued*).

tilt meters, particularly those near the injection point on the southern edge of the caldera (1, 5, 8 and 13), implying that it is not simply an artifact of local site conditions. While there was occasional rainfall over the time interval, there was no significant precipitation just prior to or during the two tests. In fact, such sporadic

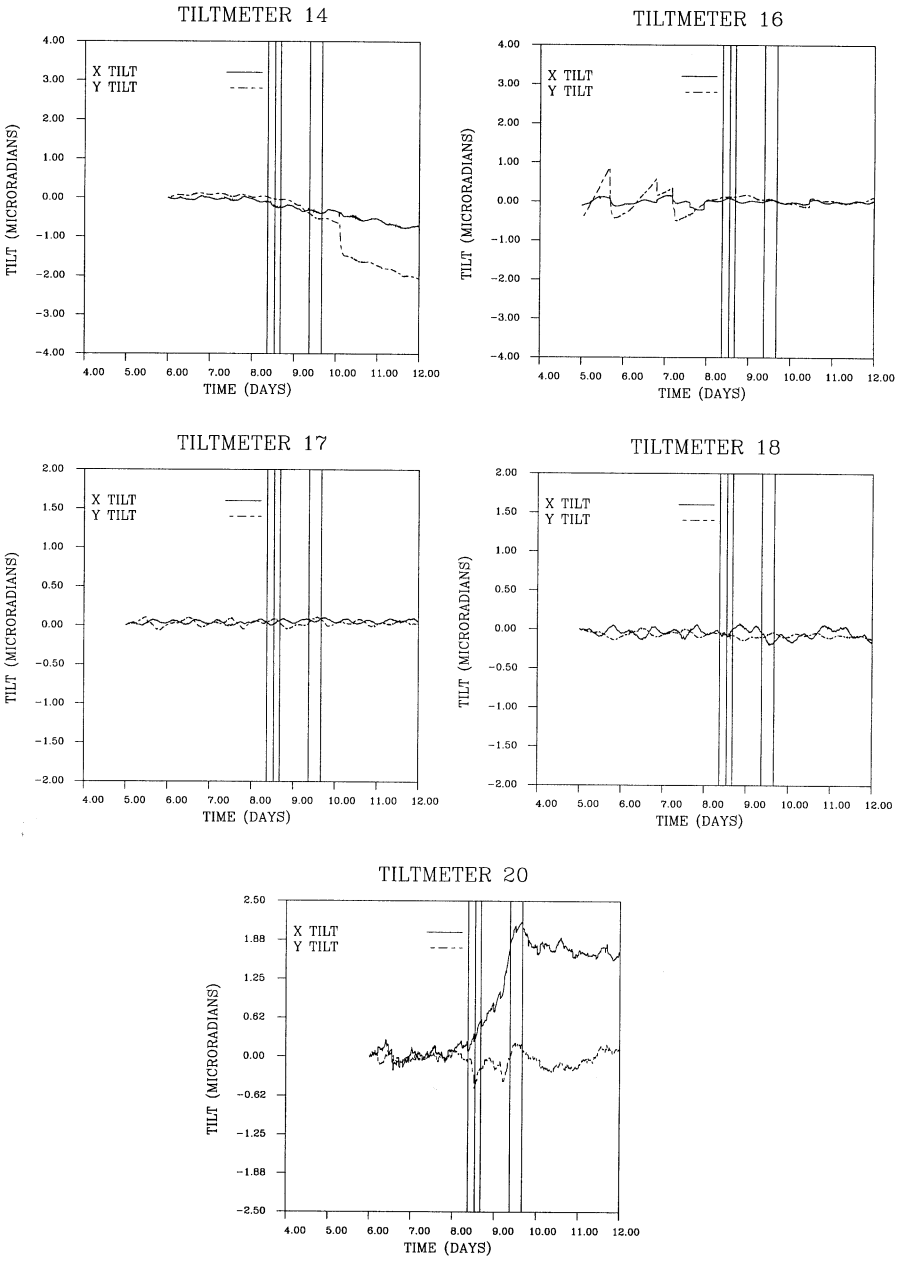

Fig. 3 (*continued*).

rainfall was normal for this time of the year, the rainy season, and had been on going for more than a month.

In an effort to better understand the possible causes of the large magnitude tilt anomaly, we consider the change in surface tilt associated with the last two days of

injection tests (Fig. 2b). That is, the surface tilt prior to the start of pumping on day eight (8.35 days) is taken as the baseline. The baseline value is subtracted from the tilt at the completion of the test on day nine (9.70 days). The result is a tilt vector, representing the change in surface tilt over the duration of the two tests (Fig. 4a). The first feature to note is the rapid spatial variation in tilt magnitude. There are large changes (over 2.0 μrad) in surface tilt at stations 1, 8, 13 and 20. However, the changes die off rapidly to the north and south of the injection location (Fig. 4a). In general, injection produces spatial variations in surface deformation of the order of the depth. This suggests that any possible volume change responsible for the surface deformation is not deep-seated.

A useful feature of tilt meter data is the dense temporal sampling. Given the one minute sampling interval of the instruments and the many days of observation (Fig. 3), it is possible to examine the variation of the surface deformation as a function of time. As an example, consider the surface tilt changes occurring after injection ceased on day 9. That is, the tilt variation from 9.7 days until 11.7 days. Note that for some tilt meters, such as 1, 5, 7, 11, 13, 14 and 20, there were significant changes in surface tilt over this time interval (Fig. 3). These changes may well be due to the re-distribution of fluid in the subsurface. The resulting change in surface tilt over this two-day interval is shown in Fig. 4b. Note the significant changes in direction at stations 1, 7 and 20. Again, the largest tilt signals are concentrated along the southern edge of the Hijiori caldera within about 0.5 km of the pumping well HDR-1. Furthermore, there is a rapid decay in tilt magnitudes away from the southern boundary of the caldera.

3.1.3. Model parameterization

The approach outlined in the Methodology section will be used in our analysis of the tilt observations. That is, the surface tilt is attributed to the injection of over 2000 barrels of water into well HDR-1. We shall solve for the fractional volume change in the subsurface that is compatible with the tilt observations. Before proceeding with an inversion for subsurface volume change the specific parameterization must be decided on. We must choose the number of layers, the depth boundaries of each layer, and the discretization of the layers (into grids of cells) that will be used in Eqs. (4) and (5). There are several issues which pertain to the choice of layer boundaries. For example, the lower boundary should span the injection interval of 2.1–2.2 km, with some allowance for deeper volume change. Because volume change may occur on dipping and intersecting fracture zones, variations in volume change with depth must be allowed. However, using many layers introduces the possibility of significant trade-off between model parameters, contributing to the non-uniqueness of the estimates. It was felt that a minimum of three layers was required for sufficient model variability with depth. The choice of the depth to the top of the model is of particular importance. The top layer should be shallow enough to represent the spatial variation in tilt observed at the surface. Furthermore, because the surface tilt magnitude decays rapidly with depth (Castillo et al., 1997), the top layer must not be too deep or it will not be possible to match the tilt magnitudes with an appropriate volume change. To gain some insight on the variation of tilt

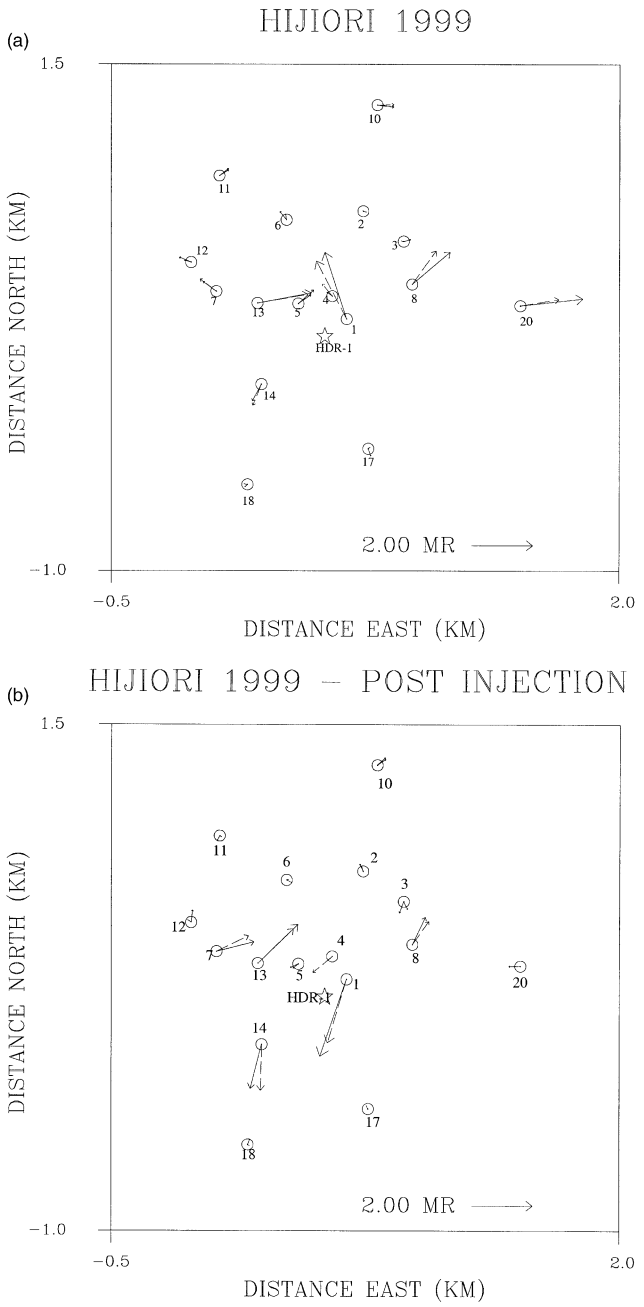

Fig. 4. (a) Vectors corresponding to changes in surface tilt between 8.35 days and 9.70 days. The observed tilt is indicated by the solid arrows. The tilts predicted by the volume change model are given by the dashed arrows. (b) Post-injection tilt vectors. The vectors correspond to changes in surface tilt between 9.70 and 11.70 days.

magnitude with depth, consider the following series of forward calculations. In each forward run a volume increase is located in a small cell centered roughly at the X–Y position of the injection well HDR-1 (Fig. 1). The volume change corresponded to the total injected volume during the experiments of day 8 and day 9, roughly 300,000 litres. We calculated the peak surface tilt observed at the array of stations, for injections at various depths (Fig. 5). Note that the tilt magnitude decays rapidly with depth, from around 2.9 μrad at a depth of 0.40 km to less than 0.3 μrad at a depth of 0.75 km. Thus, in order to satisfy the observed tilt magnitude of over 2 μrad and the rapid spatial variation in which tilt magnitudes decay rapidly over distances of several hundred meters [Fig. 4(a) and (b)], our top layer boundary was set at a depth of 0.3 km. From these considerations a model with layers 0.3–0.8, 0.8–1.8, and 1.8–2.8 km is adopted. The internal layer boundaries at 0.8 and 1.8 km depth do not correspond to any particular geologic boundaries. Each layer is sub-divided into a 30 by 30 grid of cells, resulting in block dimensions of 67 m (east-west) by 67 m (north-south).

3.1.4. Model parameter resolution. As noted above, there is some degree of non-uniqueness inherent in our model parameter estimates. For example, there may be trade-offs between volume change in the various layers of our model. We have seen that the data are less sensitive to deeper volume change and may not be able to constrain the model at depth (Fig. 5). Also, there are a large number of model parameters and many fewer data, contributing to the non-uniqueness. To quantify

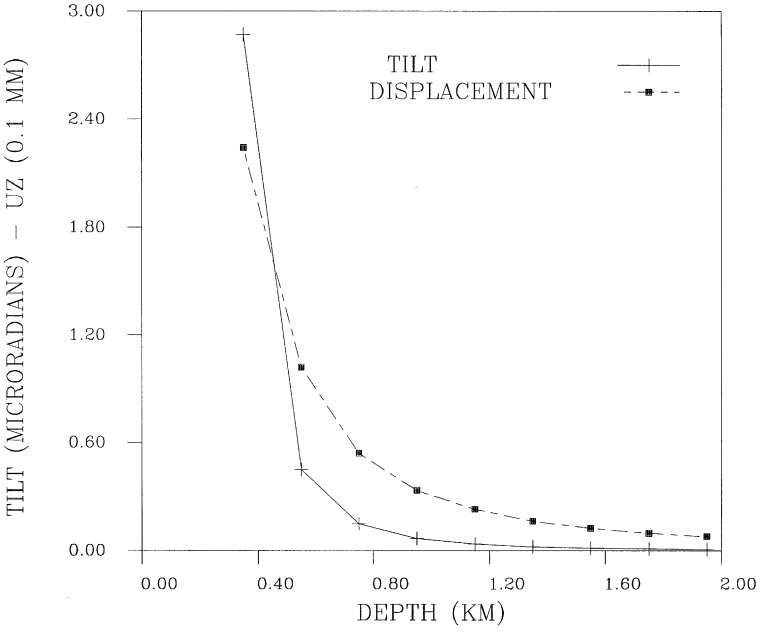

Fig. 5. Peak tilt (solid line) and surface displacement (dashed line) due to a volume change of 300,000 litres situated at various depths.

our resolution of subsurface volume change the model parameter resolution matrix was computed (Fig. 6). As noted in the Methodology section, the rows of the resolution matrix are averaging coefficients describing the contribution all model parameters make to a particular estimate. The diagonal elements of the resolution matrix measure our ability to estimate the volume change in each cell. If it is possible to determine the volume change in a block without trade-offs from other model parameters, the diagonal element for that block will be unity. If there is considerable trade-off with other model parameters the diagonal element will be close to zero. In Fig. 6 the diagonal elements of the resolution matrix are displayed. Observe that, in the uppermost layer (0.3–0.8 km), most of the values are fairly close to one, particularly near the center of the tiltmeter array. In the second layer (0.8–1.8 km) the

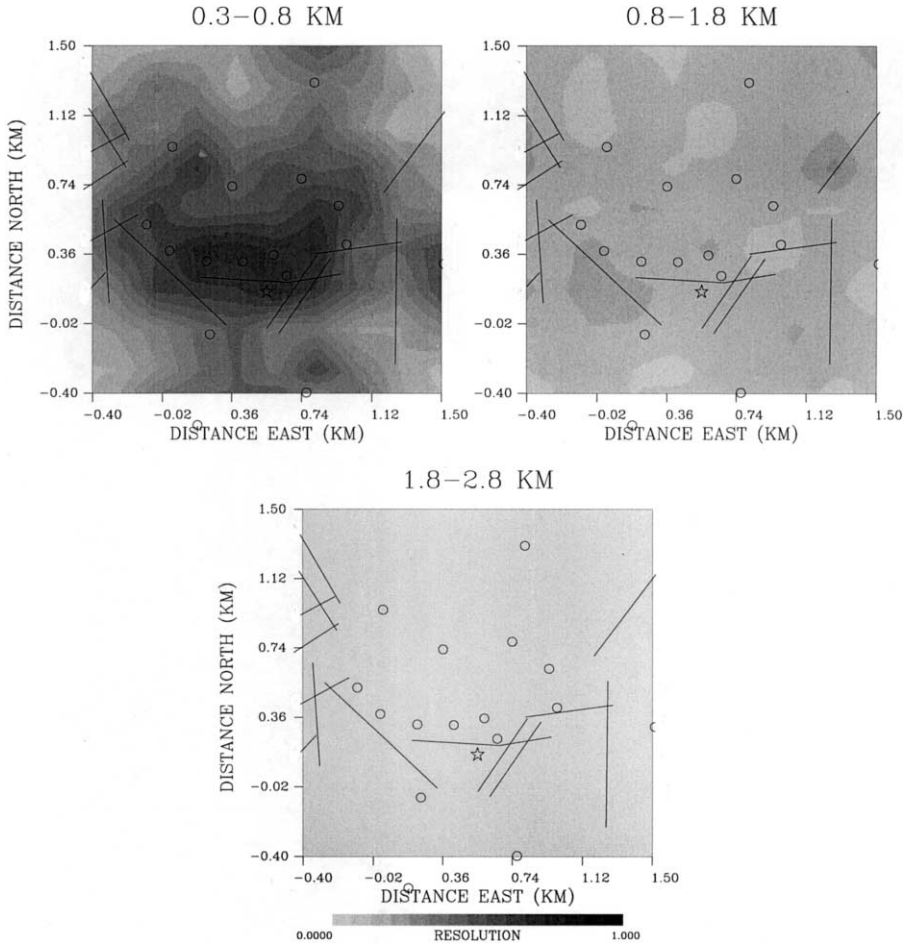

Fig. 6. Model parameter resolution estimates for the three layers of our inversion grid. The diagonal elements of the resolution matrix are displayed at the location of the corresponding grid block.

diagonal elements lie in the range 0.3–0.4 signifying lateral and vertical averaging. In the lowermost layer (1.8–2.8 km) the diagonal elements are below 0.1 and it is not possible to resolve individual block volume changes in this depth range. The variation in the diagonal elements is compatible with the rapid decay in the magnitude of surface tilt with source depth (Fig. 5). In summary, it is possible to resolve detailed features in much of the uppermost layer (0.3–0.8 km) and large-scale features in the intermediate layer (0.8–1.8 km).

3.1.5. Inversion for fractional volume change at depth. Given the three layer grid of 2700 cells we can infer the distribution of subsurface volume change that is compatible with the observed tilt data. Using the penalized least-squares approach described in Vasco et al. (1998, 2000), the misfit to the tilt data is minimized, in conjunction with the roughness of the volume change model. That is, we find the smoothest model of subsurface volume change that is compatible with the data. The resulting volume change in the two uppermost layers may be resolved. Volume changes in the lower layer (1.8–2.8 km) are not resolvable and hence not shown. There are several notable features associated with the model of volume change (Fig. 7). First, the largest volume expansions are found in the uppermost layer, concentrated in a narrow band that roughly follows the mapped ring fractures of the caldera. In fact, the two largest volume increases are located near intersections of mapped ring fractures. Secondly, much of the volume expansion is to the east of injection well HDR-1, in agreement with inferences derived from acoustic emission data and the circulation tests. Fractional volume change is observed in the depth range 0.8–1.8 km, to the south and east of the injection well HDR-1. Note that the fractional volume change in this layer is sensitive to the regularization and only moderately resolvable. The fit to the data is only slightly improved by the presence of this fractional volume change. Overall, our fit to the tilt data is quite good [Fig. 4(a)], given the assumptions in our inversion, e.g. treating the caldera as a homogeneous half-space.

We also inverted the post-injection tilt observations [Fig. 4(b)] for volume change. The parameterization was identical to that used above. The largest volume change is found above 0.8 km, concentrated along the southern boundary of the caldera (Fig. 8). The westernmost component of volume change follows a northwest-trending ring fracture. There is a deeper component of volume change (0.8–1.8 km) also at the western edge of the caldera but it is extremely small and not well resolved. This component of volume change suggests the westward migration of fluid along the ring fracture zone. In general, there is a larger concentration of fractional volume change in the uppermost layer in the post-injection inversion, with less volume change at depth. That is, there is proportionally more shallow volume change (0.3–0.8 km) after the conclusion of the pumping tests (Figs. 7 and 8). For the most part the fit to the post-injection data is quite good [Fig. 4(b)]. Station 4 had the poorest fit with a much larger predicted tilt than was observed. There was also a small observed response during the injection interval [Fig. 4(a)]. It may be that the station is poorly coupled to the host rock, resulting in small surface tilt. Alternatively, our 30 by 30 grid might not be fine enough to completely capture the rapid spatial variations in volume change due to fluid migration along faults and fractures.

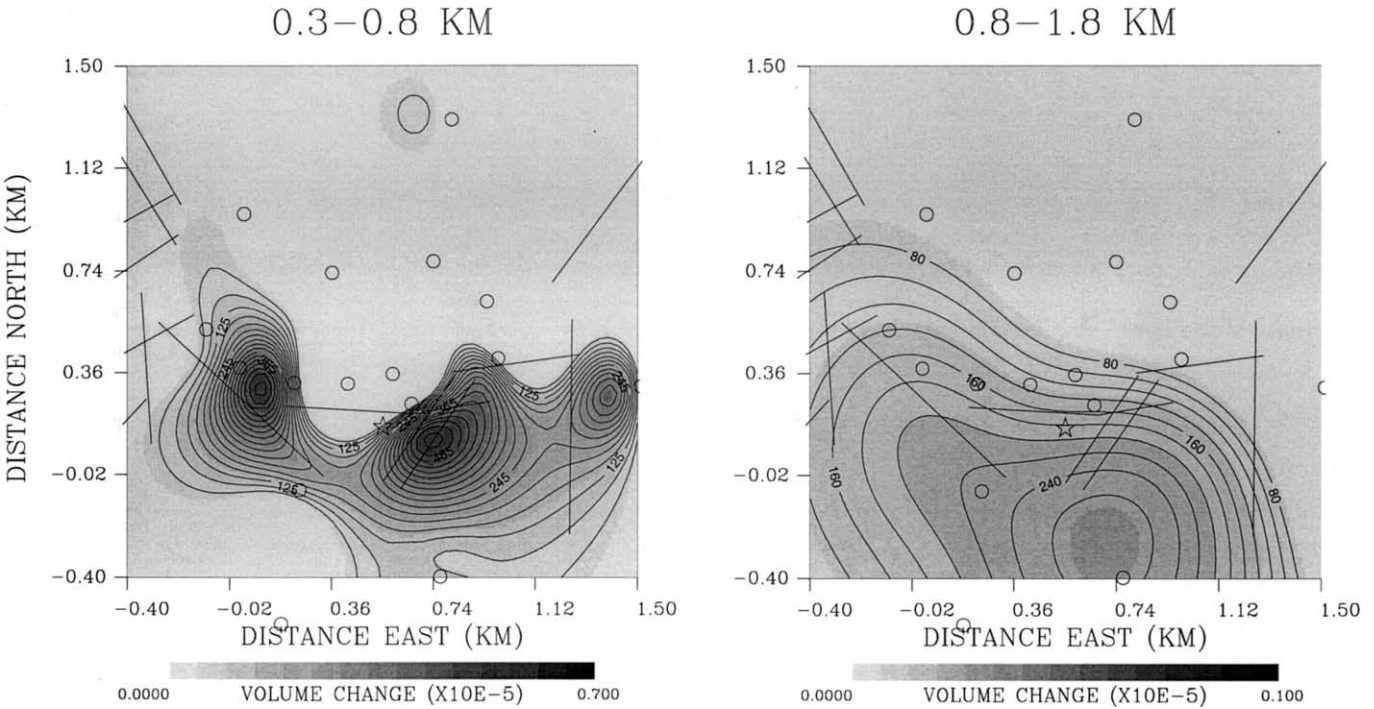

Fig. 7. Volume change for two layers of our model. The cell values have been interpolated onto a smaller grid for plotting purposes. The locations of the tilt meters are denoted by circles; the location of the injection well HDR-1 is denoted by a star. The line segments indicate the locations of the Hijiori caldera ring fractures.

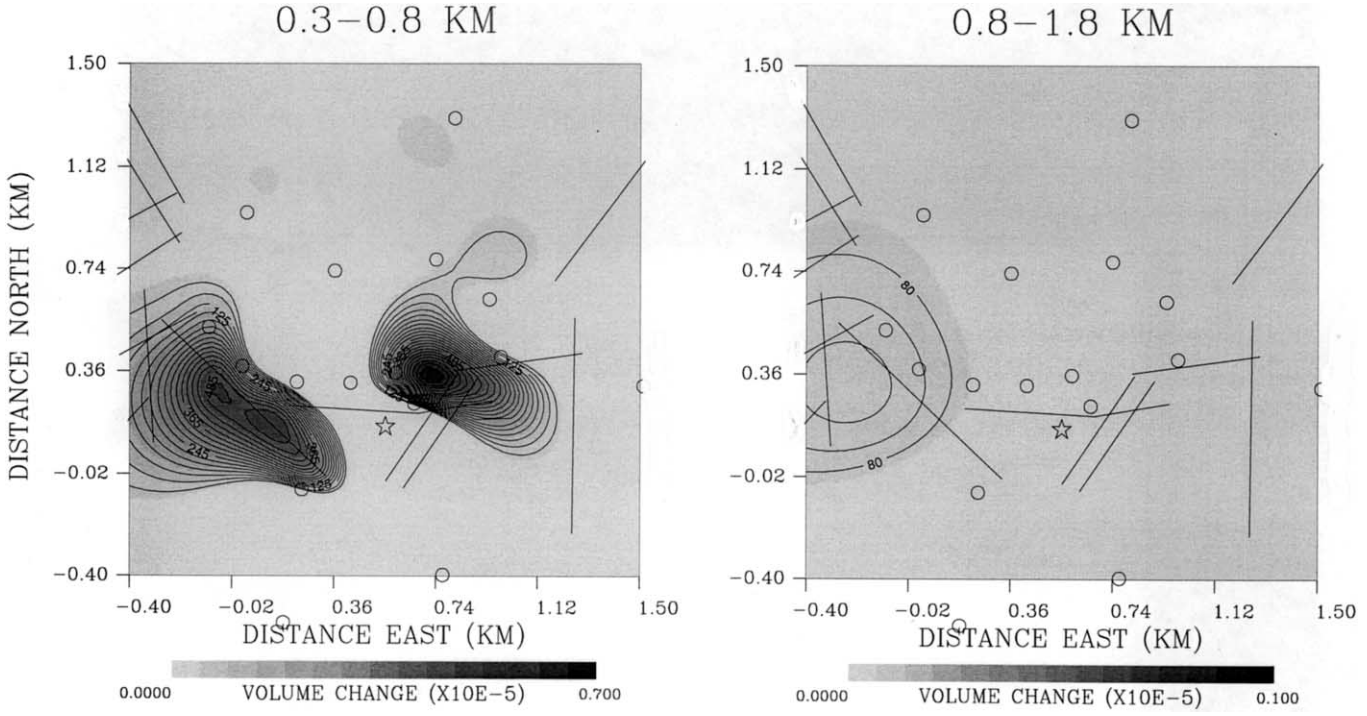

Fig. 8. Volume change for the two top layers of our post-injection model.

It is curious that the volume changes necessary to explain the large variations in surface tilt are quite shallow, 0.3–0.8 km. It may be that fluid pressure changes have migrated up the caldera ring fracture zone over time. Indeed, because the sensitivity of tilt meters decays dramatically with the depth of fractional volume change (Figs. 5 and 6), it may not be possible to image deeper reservoir volume changes. It is clear that the tilt meters can only respond to changes that are shallow enough to be detected. There are indications that fluid migration may well have commenced at depth, prior to the pumping tests on days 8 and 9. For example, at stations 7, 13 and 20 one observes a long period surface motion prior to the injection on day 8. The situation is complicated by the injection associated with the testing of the sinusoidal pumping system. Such injections continued for at least four days prior to the tilt meter experiments. Pumping cold water into the deeper fracture system will change the state of the reservoir. For example, there is evidence that the injection of cold water may increase the permeability of the fractures in the reservoir (Bodvarsson et al., 1984; Benson et al., 1987; Nakagome et al., 1994).

In an effort to explore what, if any, deeper fractional volume change may be attributed to the earlier pumping tests, an inversion of pre-test surface tilt was conducted. That is, variations in surface tilt between 5 and 8.5 days were used to image subsurface volume change. These variations capture changes that occurred before the two constant-rate tests on days 8 and 9 (Fig. 2b). In order to calculate tilt changes, all tilt observations prior to 6 days were averaged together to produce an initial estimate. This baseline value was then subtracted from the tilt measured at 8.5 days. The resulting tilt vectors are of much smaller magnitude (Fig. 9). In fact, the tilt signal is of the order of 0.1–0.2 μrad, similar in magnitude to the Earth tides. There does appear to be a coherent signal in the vectors, much like that observed in the later changes (Fig. 4a). These data were fit with deeper fractional volume changes; the layers for this inversion are 0.8–1.8 and 1.8–2.8 km in depth. Model parameter resolution calculations indicate that it is possible to resolve the fractional volume changes in the upper layer (Fig. 10). Our inversion result indicates volume change concentrated along the caldera ring fractures (Fig. 10). The southernmost volume change is to the south and east of the pumping well HDR-1, in agreement with our earlier inversion (Fig. 7). These results suggest that the testing of the sinusoidal injection system did indeed pressurize the ring fracture system in advance of the two constant-rate tests on days 8 and 9. For the most part, our model of deeper volume change is compatible with the tilt observations (Fig. 11). All but four tilt components are fit to within one standard error. However, the observations are quite noisy and the signal-to-noise ratio is fairly close to one. A major problem is the variation due to Earth tides, which is of the order 0.1–0.2 μrad. With improved processing and corrections for Earth tides, it should be possible to constrain volume changes at greater depths.

3.2. Okuaizu geothermal field

3.2.1. Geologic and geothermal setting

The Okuaizu geothermal field is located in the western part of the Aizu district of Fukushima Prefecture in northeastern Japan (Nitta et al., 1987). The regional basement

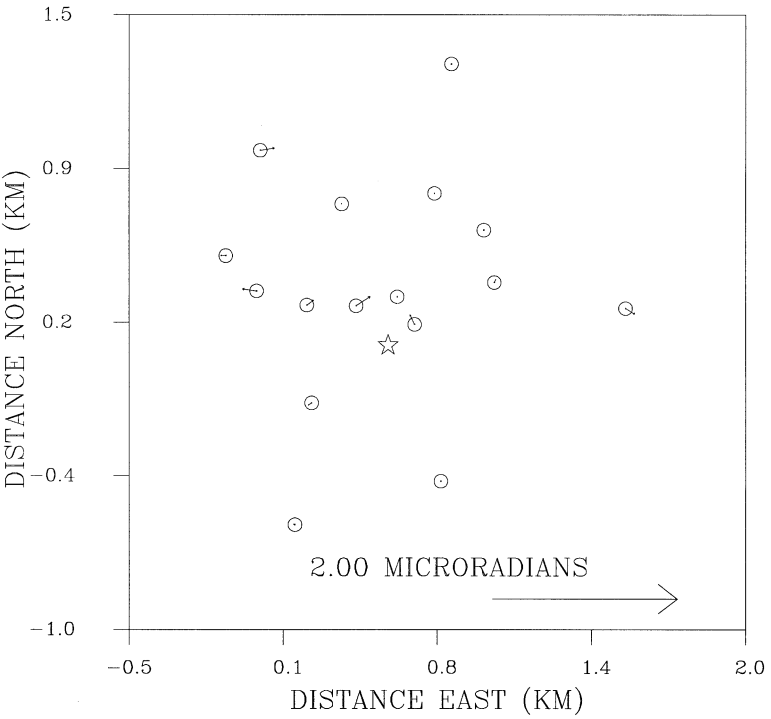

Fig. 9. Vectors corresponding to changes in surface tilt between 6.00 and 8.50 days. The observed tilt is indicated by the arrows.

consists of pre-Tertiary granodiorite and sedimentary rocks (Mizugaki, 2000) unconformably overlain by rhyolitic-to-dacitic lavas and pyroclastic and clastic rocks. These deposits are in turn overlain by caldera-related ash flow tuffs, debris avalanche deposits and lacustrine sediments. The lake sediments are extensive and occupy an area over 5 km in diameter (Mizugaki, 2000), obscuring the underlying geologic structure. The lake is hypothesized to have formed as a result of subsidence along two faults east and west of the caldera (Mizugaki, 2000). The regional basement forms an elongated basin with a secondary horst and graben structure (Nitta et al., 1987).

Several major fault and fracture zones trend to the northwest-southeast, reflecting the deep geological structure of the Okuaizu geothermal field. These include the steeply dipping Oizawa, Sarukurazawa, and Chinoikezawa fault zones (Fig. 12) (Nitta et al., 1987). There is no clear-cut relationship between these faults and the volcanic history at Okuaizu. The fault zones are truncated to the northwest by the northeasterly trending Takiyagawa fault zone. An extensive alteration halo, extending along the Takiyagawa fault zone, has been noted by Nitta et al. (1987). Such alteration, and possible 'self-sealing' along the Takiyagawa fault zone may explain the lack of significant hot springs and discharge vents within this part of the Okuaizu field (Nitta et al., 1987; Mizugaki, 2000). However, it appears that at depth much of the flow associated with the geothermal field is controlled by the northwest trending fault

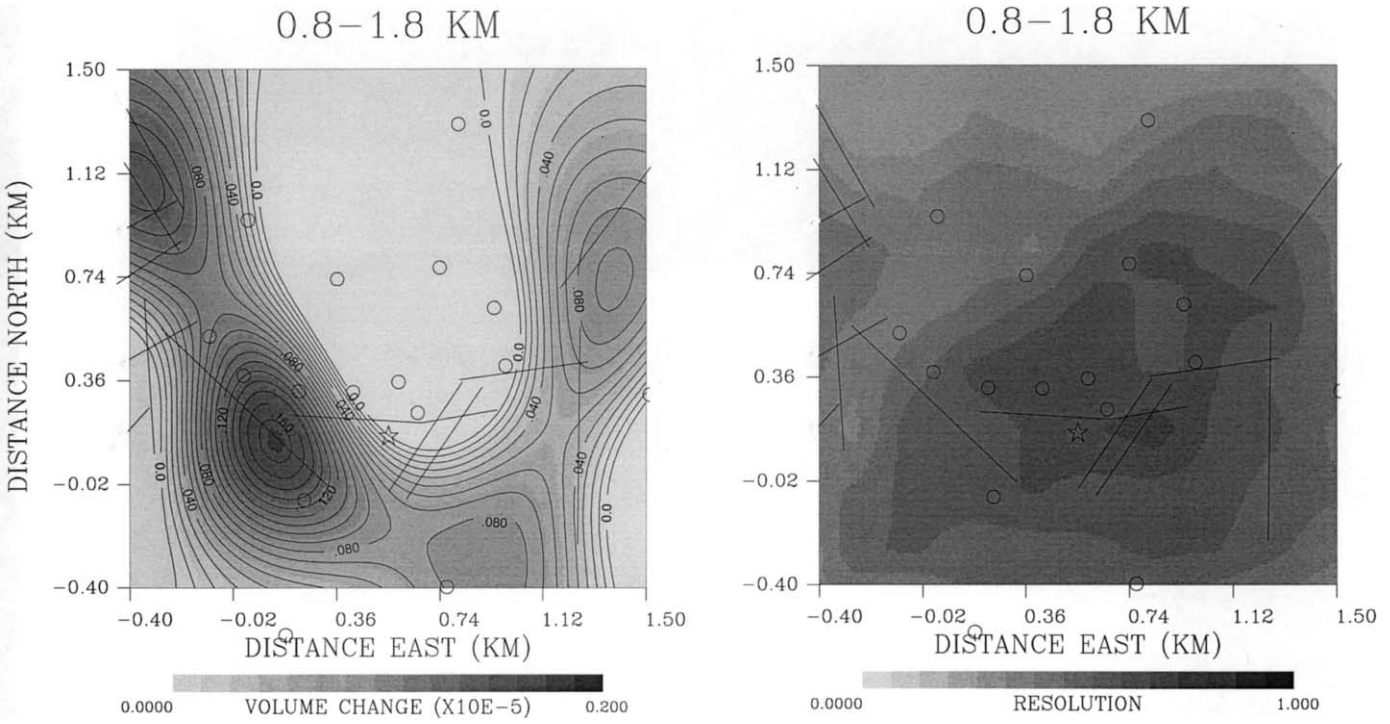

Fig. 10. (Left) Fractional volume change for the top layer of our model. (Right) Model parameter resolution estimates for the top layer of our inversion model.

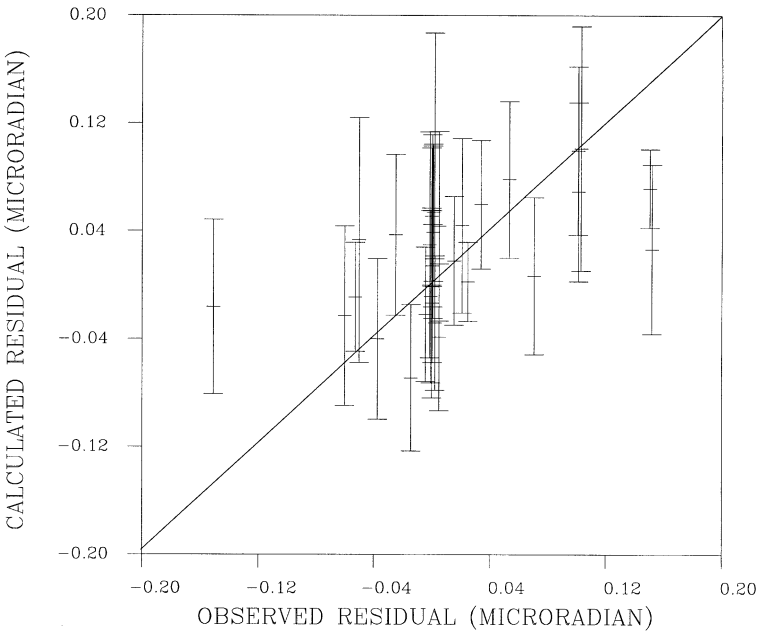

Fig. 11. Plot of observed versus calculated tilt residuals.

zones. In fact, the most productive geothermal wells intersect either the Chinoikezawa or Sarukurazawa fault zones (Mizugaki, 2000) between 1000 and 2600 m below the surface. Downhole temperature logs support the notion that the hydrothermal flow is strongly controlled by these faults (Nitta et al., 1987). Temperatures exceeding 300 °C are found between the Chinoikezawa and Sarukurazawa fault zones (1200 m below sea level), and just slightly to the southeast of the Takiyagawa fault zone. The high-temperature anomaly extends to the southeast, following the orientation of the Chinoikezawa and Sarukurazawa fault zones (Nitta et al., 1987).

Detailed surveys by the New Energy Development Organization (NEDO) in 1982 and 1983 led to the drilling of 18 exploratory wells between 660 and 2000 m in depth. The exploratory wells confirmed the existence of temperatures of more than 300 °C at 1200 m below sea level, located along the Chinoikezawa and Sarukurazawa fault zones. Since 1995 a commercial geothermal power plant, the Yanaizu-Nishiyama station with an approved capacity of 65 MW, has operated within the Okuaizu geothermal field (Osato et al., 1998). Produced fluid is reinjected to the northeast of the production zone.

A number of geophysical observations has been gathered over the geothermal field. Initial studies utilized potential field methods such as electrical and gravity surveys. The high-temperature production zone was characterized by a positive self-potential anomaly before operation of the geothermal plant. Subsequently, the anomaly disappeared, possibly due to downward geothermal flow into the reservoir (Tosha et al., 2000). Since September 1994 precision gravity surveys have been performed yearly at Okuaizu (Takemura et al., 2000). This is an effort to detect mass

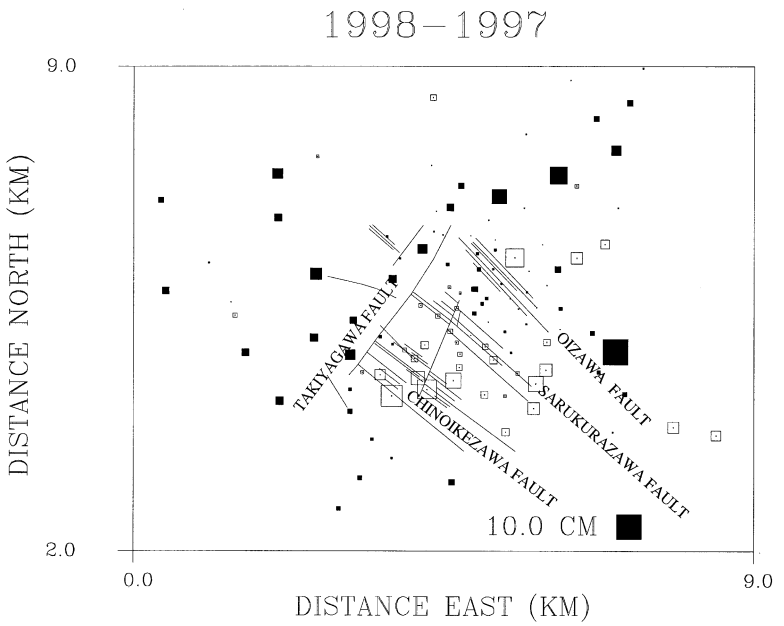

Fig. 12. Changes in elevation between two leveling surveys. The first was in the fall of 1997 and the second in the fall of 1998. Filled squares denote uplift while empty squares represent subsidence. The dimensions of each square are proportional to the magnitude of uplift or subsidence.

changes associated with the operation of the field. In 1997 the gravity network was expanded to 138 stations, covering a 30 km^2 area (Takemura et al., 2000). In support of the ongoing gravity study, leveling surveys are conducted at least yearly at all gravity stations. The leveling data are used to correct the gravity measurements for any changes in elevation.

3.2.2. Analysis of elevation changes between 1997 and 1998

In this section we examine the change in elevation that occurred during one year of operation at Okuaizu. The leveling surveys reveal systematic changes over the geothermal field between 1997 and 1998 (Fig. 12). As noted in the Methodology section, leveling data are sensitive to volume change within the geothermal reservoir. Reservoir volume increases and decreases may be induced by pressure changes and by temperature changes. In this sub-section the leveling data (Fig. 12) are used to infer the distribution of volume change within the Okuaizu reservoir. The approach is described briefly in the Methodology section and in more detail in Vasco et al. (1998, 2000).

A three-layer model is used to represent volume change within the reservoir (1.0–1.5, 1.5–2.0 and 2.0–2.5 km), covering much of the primary producing zone at Okuaizu. Each layer is subdivided into a 35 by 45 grid of cells, for a total of 4725 blocks. A total of 119 elevation changes (Fig. 12) constrain the volume change distribution at Okuaizu. In addition, both norm and roughness penalty constraints are imposed, as described in Vasco et al. (1998, 2000) in order to stabilize the inverse problem. The idea is to produce the smoothest model satisfying the observed data.

Furthermore, cells that are not required to undergo volume change in order to significantly improve the fit to the data are biased towards zero volume change. Before conducting the inversion it is important to consider our resolution of the model parameters (Fig. 13). Examining the diagonal elements of the model parameter resolution matrix, we find that the blocks in the interior of the uppermost layer (1.0–1.5 km) are quite well resolved. In addition, the fractional volume changes in the central portion of the reservoir in our second layer (1.5–2.0 km) are well constrained. Fractional volume change estimates in the lowermost layer of the model (2.0–2.5 km) are poorly determined and shall not be discussed further.

The fractional volume change estimates produced by the inversion are shown in Fig. 14. There are several interesting features in the model that may be interpreted in

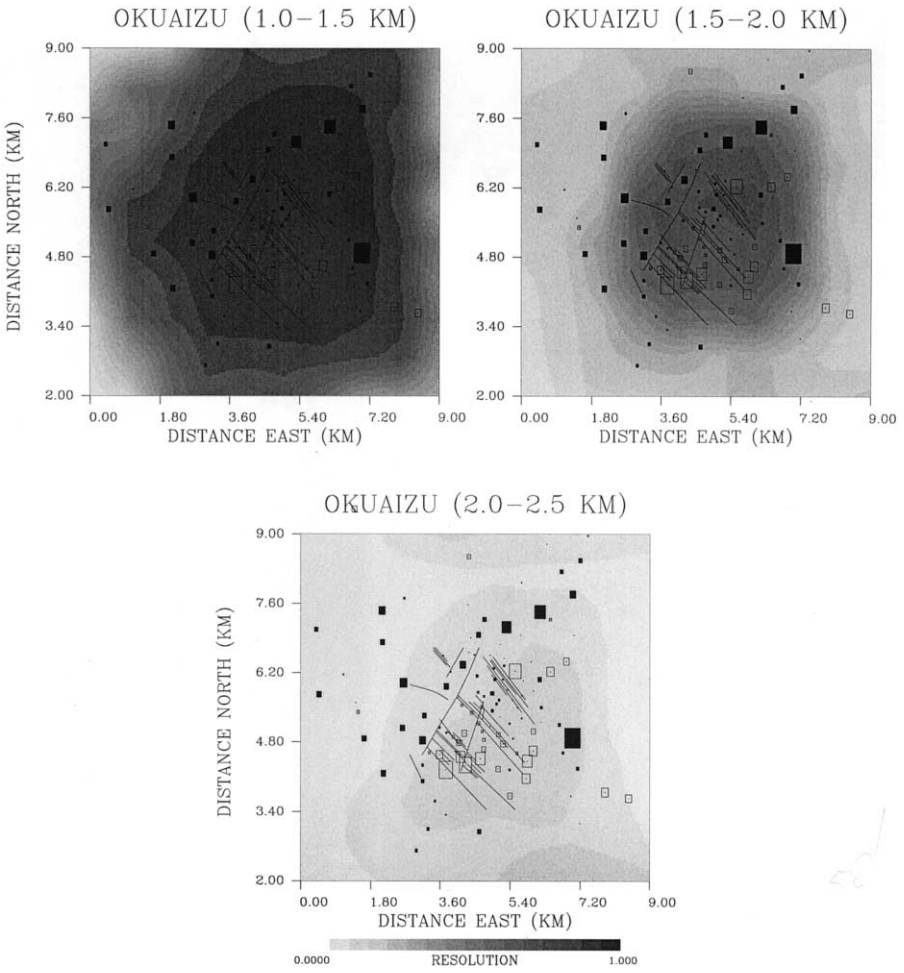

Fig. 13. Diagonal elements of the parameter resolution matrix associated with fractional volume change estimates at Okuaizu.

terms of the geothermal reservoir at Okuaizu (Fig. 14). First, the maximum volume decrease coincides with the highest subsurface temperatures, as measured in the producing wells (Osato et al., 1998). It appears that the Takiyagawa fault zone, which trends north-northeast and truncates both the Chinoikezawa and Sarukurazawa faults, does indeed act as a barrier to flow. That is, there is a systematic change in the sign of the volume change as the Takiyagawa fault zone is traversed. To the southeast there are large volume decreases, associated with geothermal production, while to the west-northwest of the fault zone a net increase in volume is observed. As noted earlier, there is evidence of an extensive alteration halo surrounding the Takiyagawa fault zone (Nitta et al., 1987), which suggests that this is a sealing fault.

The zone of volume increase, to the west of the Takiyagawa fault zone, extends up to the reinjection wells to the northeast of the production wells. There is the possibility that the injected water is migrating to the south of the Okuaizu geothermal field along the western side of the Takiyagawa fault zone. There is much less topographic relief observed above the zone of volume increase to the west, suggesting some type of geological and/or mechanical heterogeneity in the subsurface. The zone of volume decrease, which is centered on the production zone, extends for several kilometers to the southeast. The extension appears to roughly parallel the trends of the Chinoikezawa and Sarukurazawa fault zones. This extension along the faults agrees with evidence that the geothermal system is open to the southeast (Nitta et al., 1987). The Oizawa fault zone to the north, which parallels the Chinoikezawa and Sarukurazawa fault zones, does not appear to be associated with significant volume change. This may be due to a variation in flow properties; Mizugaki (2000) notes that intense alteration has occurred along the Oizawa fault zone, producing a white clay that has been mined for kaolinite. Alternatively, the absence of volume decrease near the Oizawa fault zone may be due to the lack of production wells intersecting this fault zone. The region between the Oizawa and Sarukurazawa fault zones is associated with a net volume increase and a corresponding uplift (Fig. 12). This may be due to fluid migrating from nearby injectors, which are situated around the Oizawa fault zone. Note that volume decreases are inferred to the northeast of the Oizawa fault zone (Fig. 14), a region undergoing active production.

3.2.3. Tilt meter monitoring of production changes at Okuaizu

The leveling lines at Okuaizu provide a dense network of stations. However, due to the cost of the surveys, these observation points are visited at most twice a year. Unfavorable weather in the winter, including extensive snow cover, also precludes more frequent observations for much of the year. In some situations it is necessary to record ground motion more often. In this sub-section we analyze such a situation, i.e. the transient conditions associated with geothermal field maintenance. In late May and early June of 2000, as part of a scheduled maintenance program, all production and injection within the Okuaizu geothermal field ceased. Production and injection resumed in late June and early July of the same year, approximately one month later.

In an effort to better understand the transient fluid flow associated with these changes in production and injection, an array of borehole tilt meters was deployed

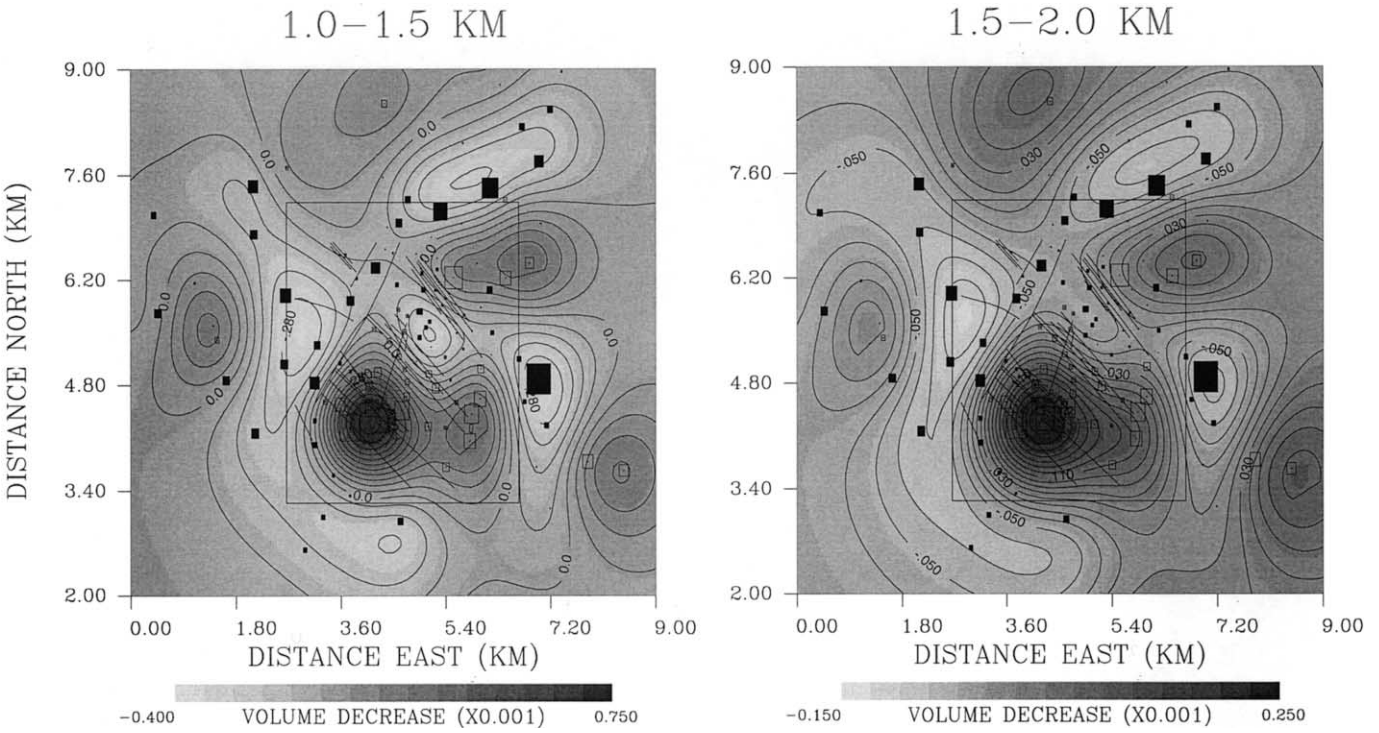

Fig. 14. Estimates of volume change in the subsurface at the Okuaizu geothermal field. The rectangles denote the elevation changes, as in Fig. 8. The faults are indicated by the solid lines. The large rectangle denotes the area modeled in the tilt inversion.

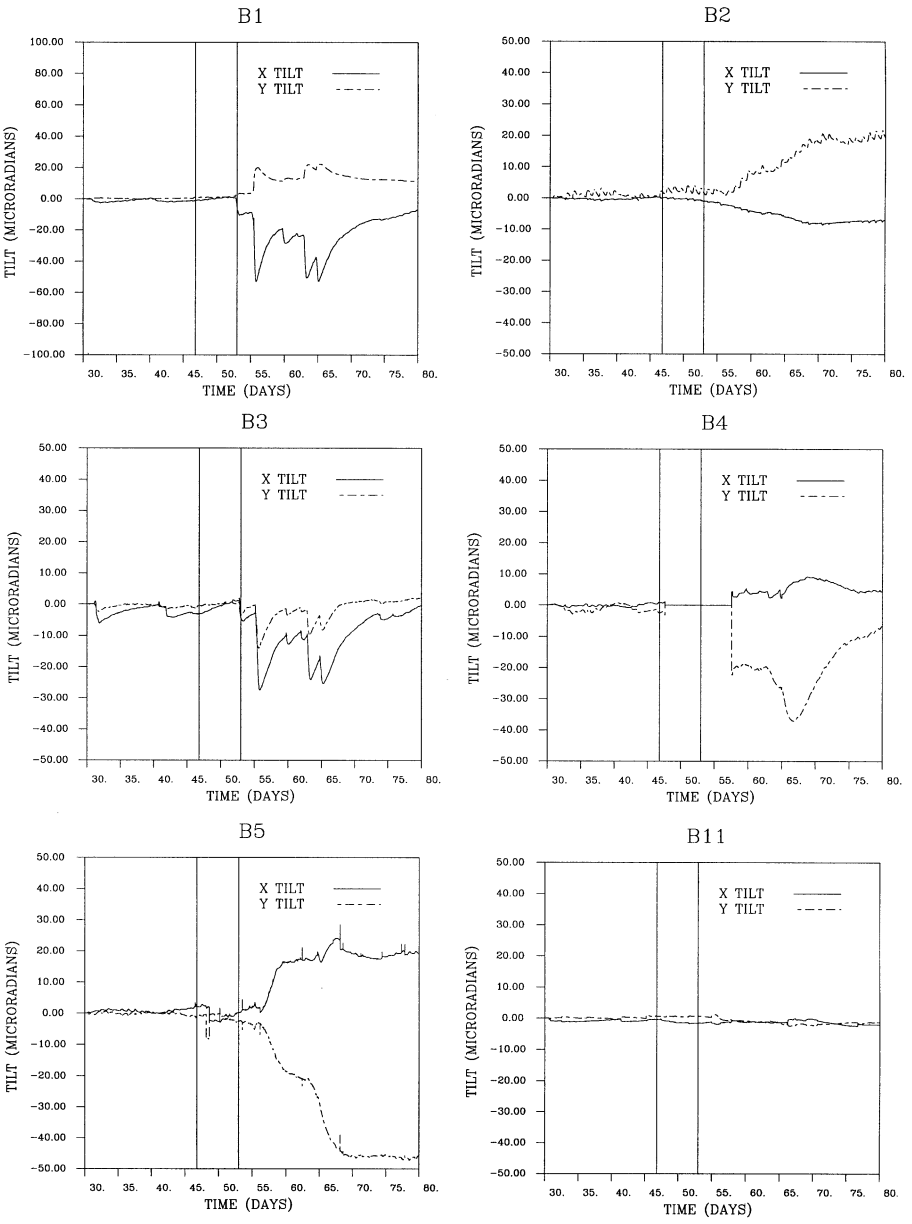

Fig. 15. X and Y components of surface tilt measured at the Okuaizu geothermal field. The first vertical line indicates the beginning of the reactivation of the producers/injectors. The next vertical line signifies when the last producer/injector was activated, after which all producers and injectors are on-line.

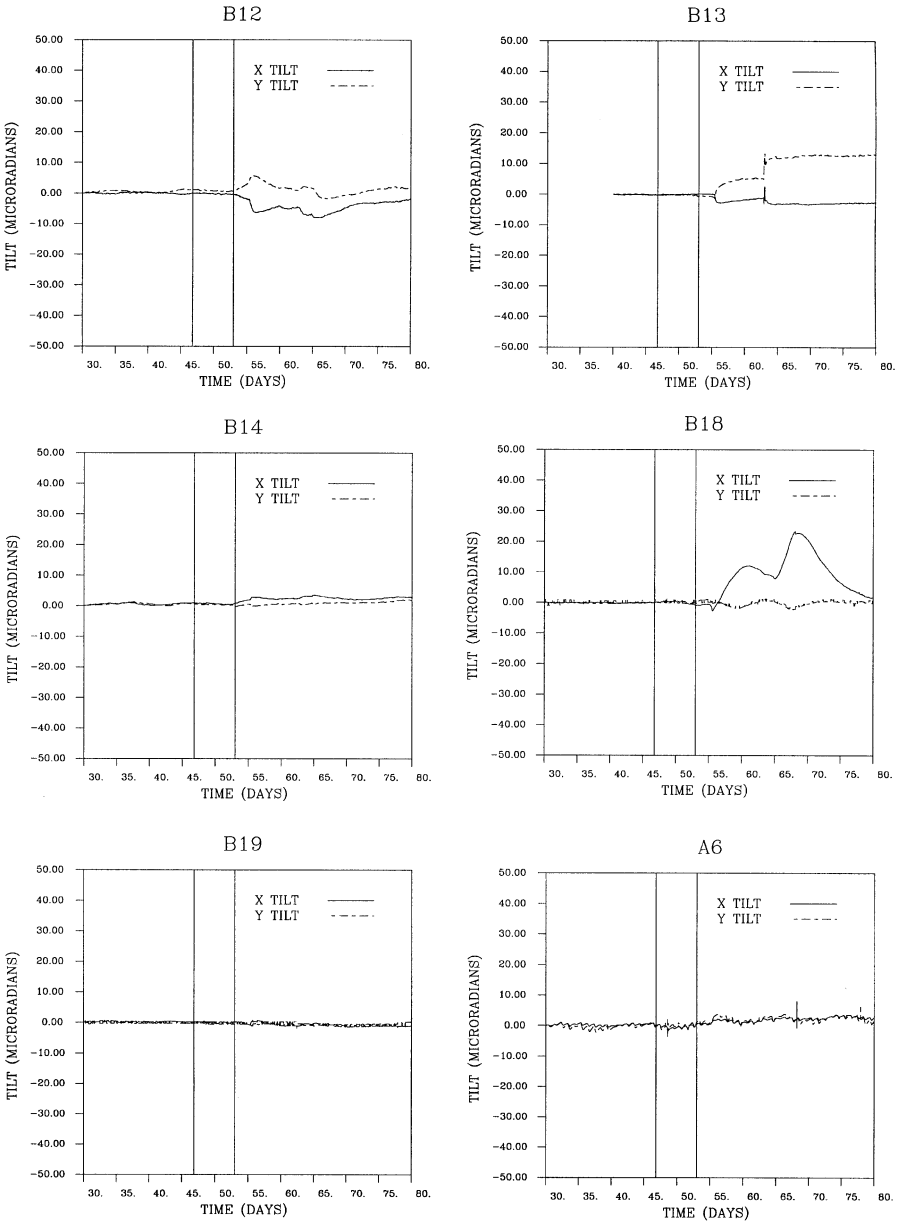

Fig. 15 (*continued*).

in and around the Okuaizu geothermal field. The station distribution was guided by the pattern of elevation change, as measured along the leveling lines. It was desirable to situate the tilt meters in the proximity of the actively producing wells, where the pressure transients are likely to be largest. Access was also a key consideration, as

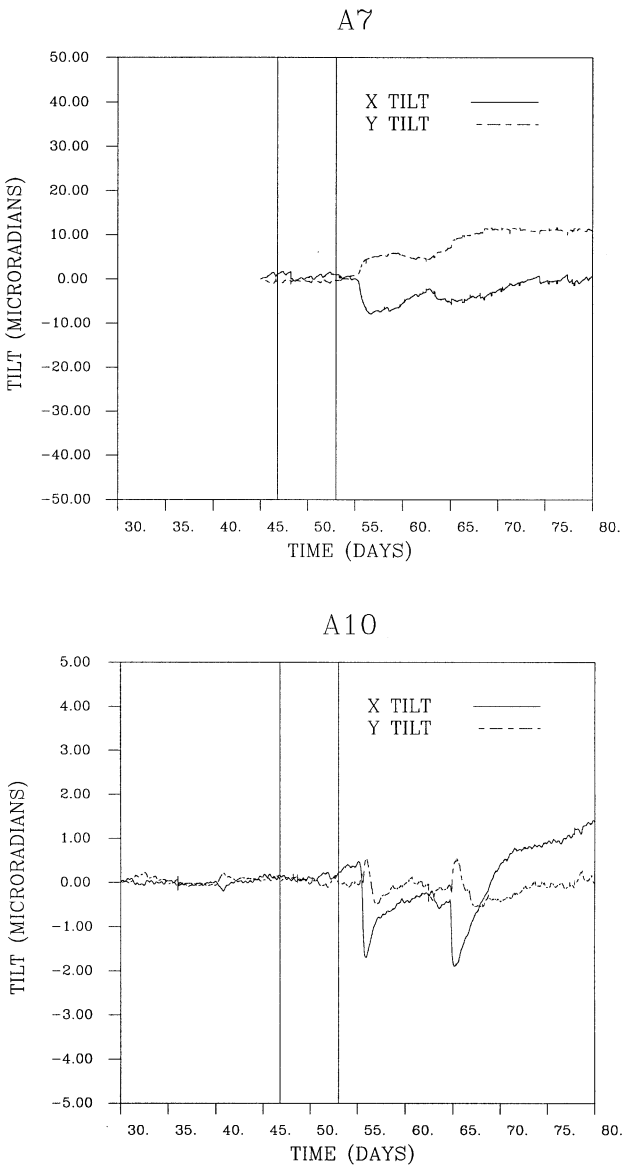

Fig. 15 (*continued*).

the tiltmeters must be emplaced in boreholes several meters deep. One difficulty was the rugged terrain overlying the zone of active production. Due to the steep topography it was only possible to site two stations near the region of peak elevation change. These stations stopped recording shortly after installation, most likely due to an insufficient supply of electrical power. Of the stations deployed, 14 operated reliably for many months following the field-wide maintenance (Figs. 15 and 16).

In this section the surface deformation associated with the resumption of field operations is considered. That is, the movement of the Earth's surface due to the start of injection and production. The time interval over which the various injectors and producers were restarted is indicated by the vertical lines (Fig. 15). Note that several stations (B1, B2, B3, B4, B5, B12, B13, B18, A7, and A10) display clear variations in surface tilt for several weeks following the resumption of injection and production. Following these transient variations most stations relax back to their orientation prior to the initiation of production and injection. Some stations, such as B2, B5, and A7, appear to have experienced permanent deformation. In order to maximize the signal-to-noise ratio, we consider the change in surface tilt from the time production resumed (47 days) until the peak deviation (64 days). The largest tilts are found in the north-central portion of the tiltmeter array (Fig. 16). Most of these stations are just south of the re-injection wells at Okuaizu, which are located around the Oizawa fault zone. The sole exception is station B1, which is just north of the injectors. Though there are large gaps in coverage, large changes in tilt, both in magnitude and direction, are observed over fairly short distances. For the most part, stations to the east and south in the array experience very little tilt. Station B18, at the extreme southern edge of the array, is an exception.

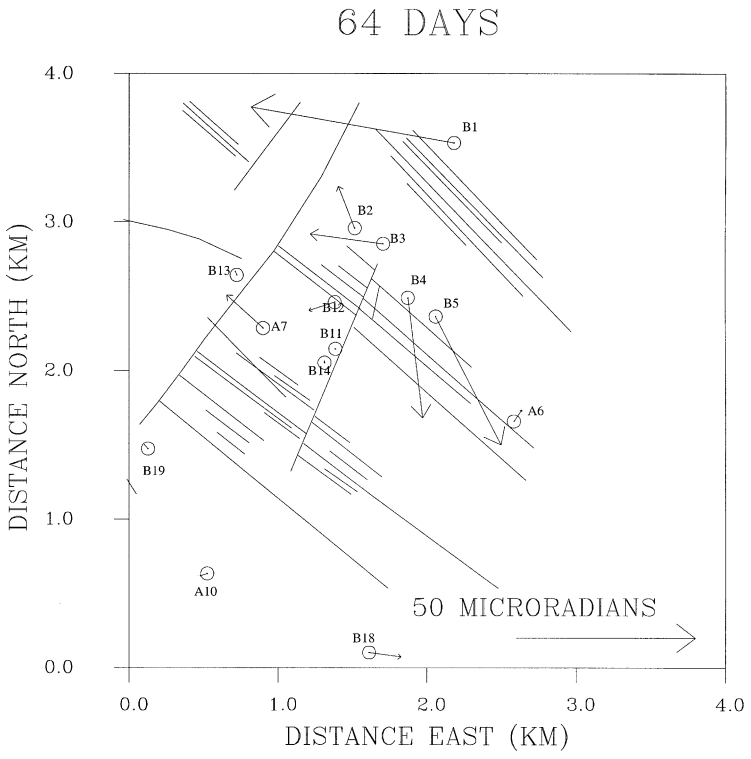

Fig. 16. Vectors corresponding to changes in surface tilt between 47 and 64 days. The observed tilt is indicated by the solid arrows.

3.2.4. Representation of reservoir volume change and inversion of surface tilt

Our representation of the subsurface fractional volume change consists of two layers, which are subdivided into 25 by 25 grids of cells. The outline of our grid is also shown for comparison with our leveling inversion result (Fig. 14). Because of the rapid spatial variation in tilt magnitude (Fig. 16), it is important to allow for shallow volume change, 0.5–1.0 km in depth. A deeper layer, 1.0–1.5 km, represents the contribution near the depth of injection. In order to determine those features of the model which are reliable, the model parameter resolution matrix was computed prior to the actual inversion. From the diagonal elements of the resolution matrix (Fig. 17) we find that fractional volume changes in the uppermost layer (0.5–1.0 km) in the central and western portion of the model are resolvable. These regions correspond to the location of the tilt meters (Fig. 16). In the deeper layer (1.0–1.5 km) only large-scale variations in fractional volume change can be determined, and the resolution is of the order of 0.3–0.5 for much of the layer.

We can take advantage of the dense sampling in time, surface tilt is measured every minute, to construct a detailed image of the response to the initiation of injection and production at Okuaizu. To this end, six regularized inversions for fractional volume change were conducted, each spanning a different time interval. The time intervals are many days apart, covering a period of 28 days (from 52 to 80 days). The results are shown for the two layers of our model, 0.5–1.0 and 1.0–1.5 km in depth (Fig. 18). All tilt variations are with respect to a baseline at 47 days. Initially, up to about 52 days, little volume change is detected by the tilt meters. Around 54 days a change in volume is observed just to the north of the injectors (the Oizawa fault zone). A narrow component of volume strain extends to the west and slightly to the south of the main volume increase. By 64 days the narrow south-trending feature appears to follow a minor fault that runs sub-parallel to the Takiyagawa fault. Furthermore, there is a slight volume increase at the southern end of our grid, near station B18. The volume strain along this fault continues for several days. After 68 days the volume increase at the northernmost edge of our grid, near the injectors, begins to decrease in magnitude. By 80 days the northernmost volume strain has almost disappeared. Furthermore, by 72 days the along-fault volume strain has broken up into two components. Each of these components appears to be associated with the intersection of the fault with the Chinoikezawa and Sarukurazawa fault zones. Perhaps the permeability is higher at the fault intersections and fluid flows preferentially upward in these regions. The pattern of volume change is suggestive of fluid migration to the south along a north-northeasterly trending fault. The appearance of volume strain at the far south of our grid, before there is a connection in our shallow (0.5–1.0 km) layer, suggests a deeper migration as well.

There is an interesting response by the southernmost tilt meter B18 that may relate to our volume change models. Station B18 has a fairly large tilt signal, similar in pattern to station B1 (Fig. 15). In fact, the time variation observed at B18 looks like a delayed and diffused variation of the variation at B1 (Fig. 19). It is possible that the tilt signal at B18 represents propagation from the injectors, down a fault zone, to the southern edge of the Okuaizu field. Such a migration may also explain why the tilt vector at B18 points almost due east. Those tilt meters that display a similar time

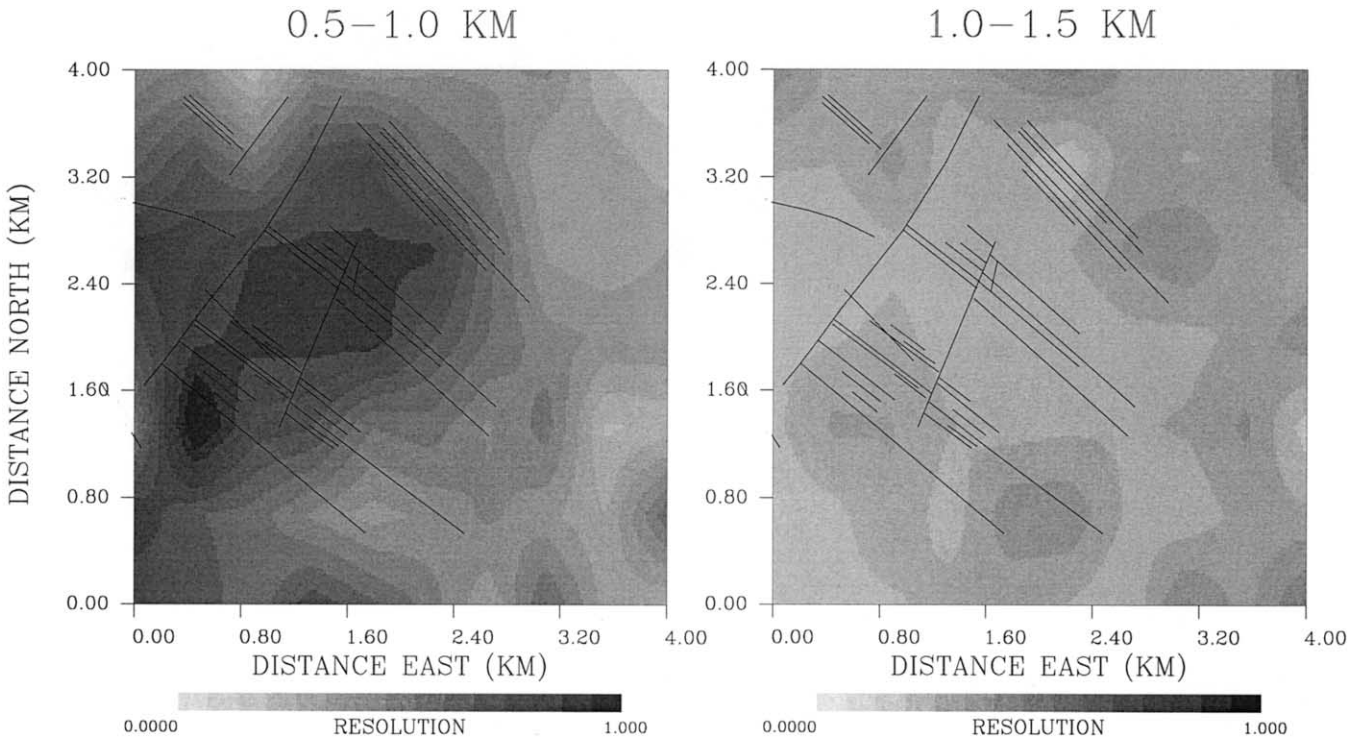

Fig. 17. Diagonal elements of the resolution matrix associated with estimates of fractional volume change.

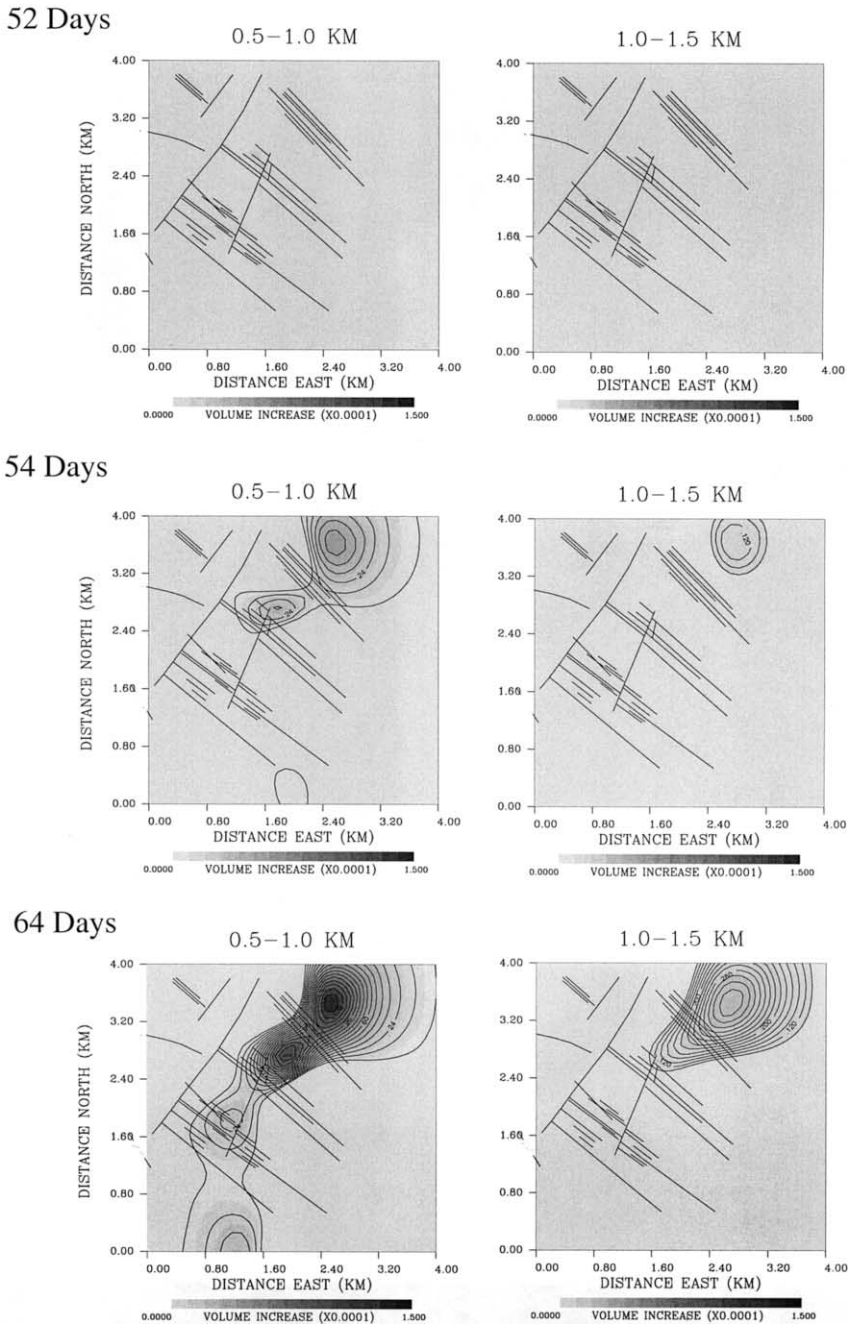

Fig. 18. Series of inversions for the volume strain over six different time intervals. The major fault zones are indicated by the thin lines.

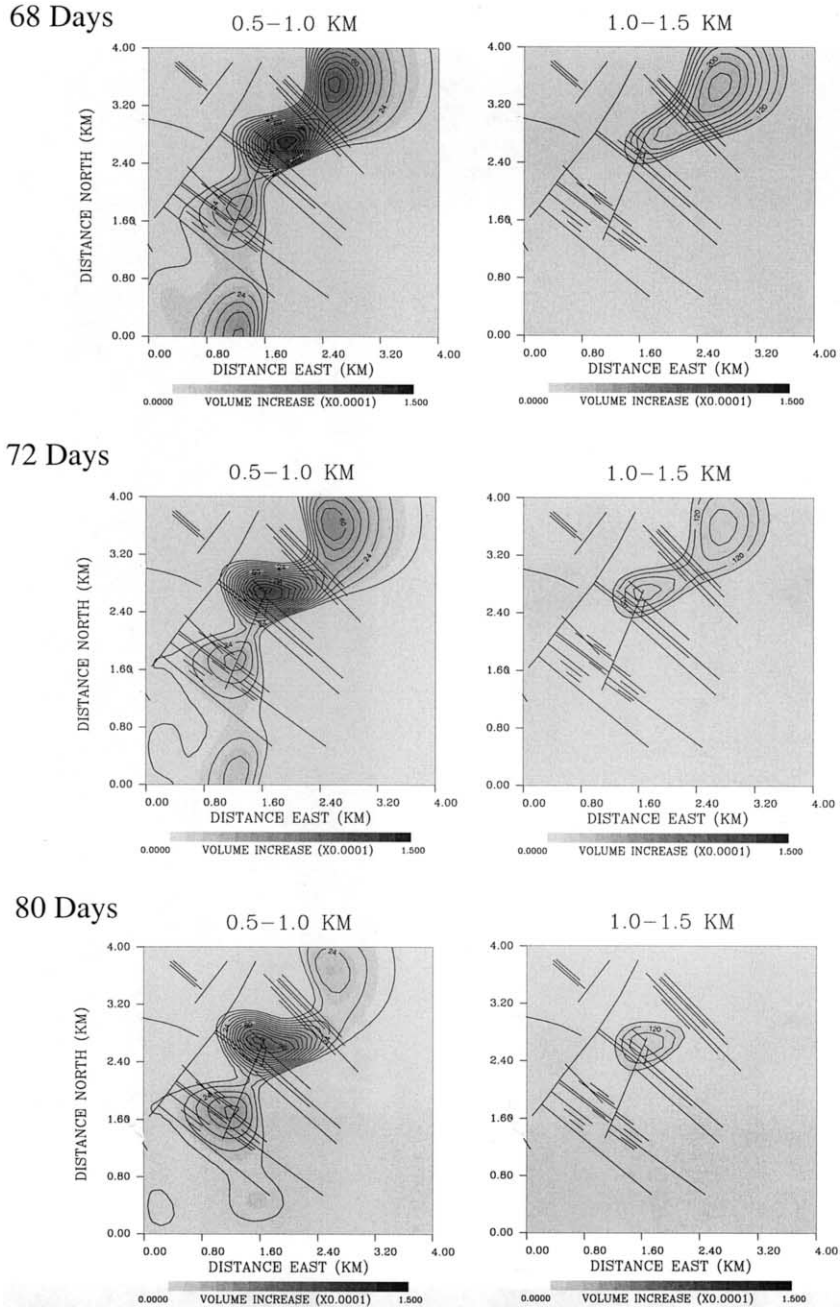

Fig. 18 (*continued*).

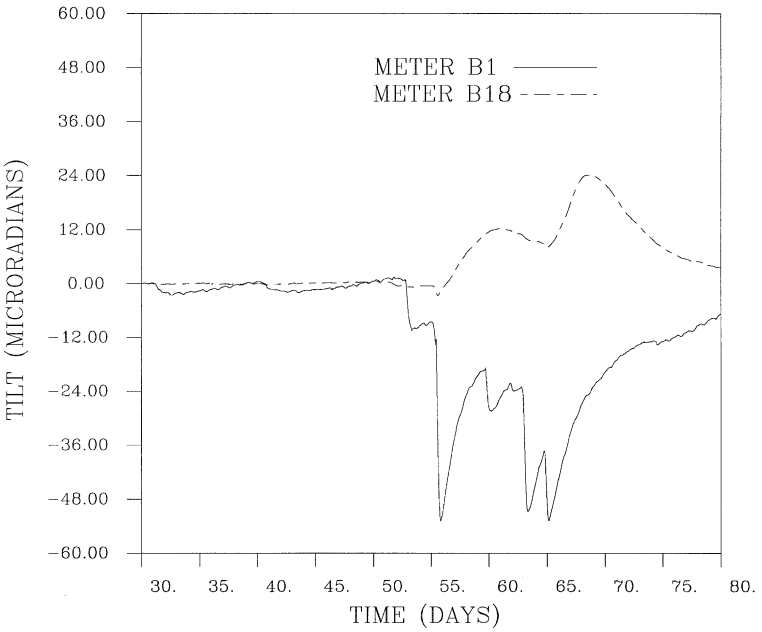

Fig. 19. X components from tilt meters B1 and B18.

history, with two notable pulses, lie along a linear trending line that parallels the Takiyagawa fault. Note that the tilt signals associated with these particular instruments relax back to the background values after several weeks. Thus, it appears that the signal is transient in nature and not part of the long-term surface deformation.

In large measure, the leveling and tilt data are indeed complementary. For example, both data sets imply volume increase at depth, in a region situated between the Oizawa and Sarukurazawa fault zones. Also, the inversion results from leveling and tilt both support the notion that the Takiyagawa fault acts as a barrier to flow along the Chinoikezawa and Sarukurazawa fault zones. When viewed together, the data suggest interesting transient and long-term patterns of flow at the Okuaizu geothermal field. The tilt data provide evidence that some faults may propagate fluid on a fairly short time scale. This propagation is transient, however, and may be related to the pressure build-up associated with re-starting injection at Okuaizu. More work is necessary before definitive statements with regard to the flow paths within the reservoir are possible. For example, it would be interesting to examine well pressures and micro-seismic activity in conjunction to surface deformation.

4. Discussion and conclusions

The results of this study indicate that fluid movement within geothermal environments gives rise to observable surface deformation. This finding is supported by numerous other investigations documenting surface displacements above geothermal

fields. Deformation has even been mapped from space using InSAR observations (Vadon and Sigmundsson, 1997; Massonnet et al., 1997; Carnec and Fabriol, 1999; Fialko and Simons, 2000; Vasco et al., 2001a). Using tilt meters it is possible to image rapid surface deformation caused by transient conditions such as well tests and production and injection changes. The observations confirm the importance of faults and fractures in subsurface fluid flow. In particular, the intersections of fault and fracture zones appear to act as conduits for flow in the geothermal areas studied here. Currently, surface deformation data are a tool for exploratory studies of fluid flow in reservoirs. That is, these data are useful for inferring gross properties of flow and for developing conceptual models of reservoir flow structure. There are several questions that need to be addressed by additional study. For example, the role of mechanical heterogeneity in concentrating deformation along fault zones. Specifically, the increased deformation near fault and fracture zones may be related to the fact that these are weak regions which deform more easily when subjected to pressure changes. There may well be a coupled effect in which higher permeability and weak mechanical properties reinforce each other to amplify deformation at fault zones.

The results of this study highlight the usefulness of surface displacements in monitoring geothermal field operations. However, these results are preliminary and one can extend this work in several respects. It is possible to combine geodetic and pressure data to image reservoir pressure variations (Vasco et al., in press b). In favorable situations we can take the analysis a step further and infer permeability variations within the reservoir (Vasco et al., in press b). It is also possible to combine various types of displacement data, such as leveling, tilt, Interferometric Synthetic Aperture Radar (InSAR) and Global Positioning System (GPS) observations, to better constrain subsurface volume changes. As discussed in Dieterich and Decker, (1975), combining the various components of surface displacement better constrains subsurface volume changes. These developments will further enhance our ability to image fluid movement using geodetic observations.

Acknowledgements

This work was supported by JAPEX of Japan. The authors would like to thank Pinacle Technologies for providing the borehole tilt meters. Thanks are also extended to two anonymous reviewers for their careful work. All computations were carried out at the Center for Computational Seismology, Berkeley Laboratory.

References

Aki, K., Richards, P.G., 1980. Quantitative Seismology. Freeman and Sons.

Allis, R.G., 2000. Review of subsidence at Wairakei field, New Zealand. Geothermics 29, 455–478.

Benson, S.M., Daggett, J.S., Iglesias, E., Arellano, V., Ortiz-Ramirez, J., 1987. Analysis of thermally induced permeability enhancement in geothermal injection wells. 12th Workshop on Geothermal Reservoir Engineering, Stanford University, pp. 57–65.

Bodvarsson, G.S., Benson, S.M., Sigurdsson, O., Stefansson, V., Eliasson, E.T., 1984. The Krafla geothermal field, Iceland 1. Analysis of well test data. Water Resources Research 20, 1515–1530.

Bruno, M.S., Bilak, R.A., 1994. Cost-effective monitoring of injected stream migration using surface deformation analysis. Proceedings Society of Petroleum Engineering Western Regional Meeting, Society of Petroleum Engineering No. 27888, pp. 397–412.

Carnec, C., Fabriol, H., 1999. Monitoring and modeling land subsidence at Cerro Prieto geothermal field, Baja California, Mexico, using SAR interferometry. Geophysical Research Letters 26, 1211–1214.

Castillo, W., Hunter, S., Harben, P., Wright, C., Conant, R., Davis, E., 1997. Deep hydraulic fracture imaging: recent advances in tiltmeter technologies. International Journal of Rock Mechanics and Mining Science 34, 3–4.

Denlinger, R.P., Isherwood, W.P., Kovach, R.L., 1981. Geodetic analysis of reservoir depletion at The Geysers steam field in northern California. Journal of Geophysical Research 86, 6091–6096.

Dieterich, J.H., Decker, R.W., 1975. Finite element modeling of surface deformation associated with volcanism. Journal of Geophysical Research 80, 4094–4102.

Du, Y., Aydin, A., Murdoch, L., 1993. Incremental growth of a shallow hydraulic fracture at a waste remediation site, Oakbrook, Illinois from inversion of elevation changes. International Journal of Rock Mechanics and Mining Science 30, 1273–1279.

Dussealt, M.B., Bilak, R.A., Rothenburg, L., 1993. Inversion of surface displacements to monitor in-situ processes. International Journal of Rock Mechanics and Mining Science 30, 1219–1222.

Eshelby, J.D., 1957. The determination of the elastic field of an ellipsoidal inclusion, and related problems. Proceedings of the Royal Society of London, Series A 241, 376–396.

Evans, K.F., Holzhausen, G.R., Wood, M.D., 1982. The geometry of a large-scale nitrogen gas hydraulic fracture formed in Devonian shale: an example of fracture mapping using tiltmeters. Society of Petroleum Engineering Journal 22, 755–763.

Fialko, Y., Simons, M., 2000. Deformation and seismicity in the Coso geothermal area, Inyo County, California: observations and modeling using satellite radar interferometry. Journal of Geophysical Research 105, 21 781–21 793.

Fielding, E.J., Blom, R.G., Goldstein, R.M., 1998. Rapid subsidence over oil fields measured by SAR interferometry. Geophysical Research Letters 25, 3215–3218.

Galloway, D.L., Hudnut, K.W., Ingebritsen, S.E., Phillips, S.P., Peltzer, G., Rogez, F., Rosen, P.A., 1998. Detection of aquifer system compaction and land subsidence using interferometric synthetic aperture radar, Antelope Valley, Mojave, Desert, California. Water Resources Research 34, 2573–2585.

Golub, G.H., Van Loan, C.F., 1989. Matrix Computations. Johns Hopkins University Press, Baltimore.

Hatton, J.W., 1970. Ground subsidence of a geothermal field during exploitation. Geothermics 2, 1294–1296. (special issue 2).

Hoffmann, J., Zebker, H.A., Galloway, D.L., Amelung, F., 2001. Seasonal subsidence and rebound in Las Vegas Valley, Nevada, observed by synthetic aperture radar interferometry. Water Resources Research 37, 1551–1566.

Kitani, S., Miyairi, M., Tezuka, K., Yagi, M., 1998. Geologic structure in and around Hijiori HDR test site. Proceedings of the 4th International Hot Dry Rock Forum, Strasbourg.

Kruger, P., Yamaguchi, T., 1993. Thermal drawdown analysis of the Hijiori HDR 90-day circulation test. Eighteenth Workshop on Geothermal Reservoir Engineering, Stanford University, pp. 111–118.

Kuriyagawa, M., Tenma, N., 199. Development of hot dry rock technology at the Hijiori test site. Geothermics 28, 627–636.

Langbein, J.O., 1981. An interpretation of episodic slip on the Calaveras fault near Hollister, California. Journal of Geophysical Research 86, 4941–4948.

Lofgren, B.E., 1987. Monitoring crustal deformation in the Geysers-Clear Lake geothermal system, California. US Geological Survey Open File Report 78–597.

Maruyama, T., 1964. Statical elastic dislocations in an infinite and semi-infinite medium. Bulletin of the Earthquake Prevention Research Institute of the University of Tokyo 42, 289–368.

Massonnet, D., Holzer, T., Vadon, H., 1997. Land subsidence caused by East Mesa geothermal field, California, observed using SAR interferometry. Geophysical Research Letters 24, 901–904.

Menke, W., 1989. Geophysical Data Analysis: Discrete Inverse Theory. Academic Press, Orlando.

Mizugaki, K., 2000. Geologic structure and volcanic history of the Yanaizu-Nishiyama (Okuaizu) geothermal field, Northeast Japan. Geothermics 29, 233–256.

Mogi, K., 1958. Relations between the eruptions of various volcanoes and the deformations of the ground surfaces around them. Bulletin of the Earthquake Research Institute 36, 99–134.

Mossop, A., Segall, P., 1999. Volume strain within The Geysers geothermal field. Journal of Geophysical Research 104, 29113–29131.

Nakagome, O., Ishii, Y., Muraoka, H., 1994. Fracture characterization of the geothermal reservoir inferred from pressure transient data. Transactions of the Geothermal Research Council 18, 591–597.

Narasimhan, T.N., Goyal, K.P., 1984. Subsidence due to geothermal fluid withdrawal, in man-induced-land subsidence. Rev. Eng. Geol., Vol. 6. Geological Society of America, Boulder, CO, pp. 35–66.

Nitta, T., Suga, S., Tsukagoshi, S., Adachi, M., 1987. Geothermal resources in the Okuaizu, Tohoku district, Japan. Chinetsu 24, 26–56.

Osato, K., Sato, T., White, S., Burnell, J., Yokomoto, S., 1998. Development of an integrated geothermal reservoir modeling system. Twenty-Third Workshop on Geothermal Reservoir Engineering, Stanford University, pp. 1–9.

Palmer, I.D., 1990. Uplifts and tilts at Earth's surface induced by pressure transients from hydraulic fractures. Society of Petroleum Engineering Prod. Eng. 25, 324–332.

Parker, R.L., 1994. Geophysical Inverse Theory. Princeton University Press, Princeton.

Savage, J.C., Clark, M.M., 1982. Magmatic resurgence in Long Valley caldera, California: possible cause of the 1980 Mammoth Lakes earthquakes. Science 217, 531–533.

Segall, P., Harris, R., 1987. Earthquake deformation cycle on the San Andreas fault near Parkfield, California. Journal of Geophysical Research 92, 10511–10525.

Stancliffe, R.P.W., van der Kooij, M.W.A., 2001. The use of satellite-based radar interferometry to monitor production activity at the Cold Lake heavy oil field, Alberta, Canada. American Association of Petroleum Geologists Bulletin 85, 781–793.

Swenson, D., Schroeder, R., Shinohara, N., Okabe, T., 1999. Analysis of the Hijiori long term circulation test. Twenty-Fourth Workshop on Geothermal Reservoir Engineering, Stanford University, pp. 344–351.

Takemura, T., Shiga, N., Yokomoto, S., Saeki, K., Yamanobe, H., 2000. Gravity monitoring in Yanaizu-Nishiyama geothermal field, Japan. World Geothermal Congress 2000 Abstracts, Kyushu-Tohoku, Japan, May, p. 50.

Tenma, N., Ikawa, T., Masahiro, N., 1997. Productivity of a recent three-well system at Hijiori HDR Test Site. Twenty-Second Workshop on Geothermal Reservoir Engineering, Stanford University, pp. 191–194.

Tosha, T., Ishido, T., Matsushima, N., Nishi, Y., 2000. Self-potential variation in the Yanaizu-Nishiyama geothermal field and its interpretation by the numerical simulation. World Geothermal Congress 2000 Abstracts, Kyushu-Tohoku, Japan, p. 48.

Vadon, H., Sigmundsson, F., 1997. 1992-1995 crustal deformation at Mid-Atlantic ridge, SW Iceland, mapped by radar interferometry. Science 275, 193–197.

Vasco, D.W., Johnson, L.R., Goldstein, N.E., 1988. Using surface displacement strain observations to determine deformation at depth with an application to Long Valley Caldera California. Journal of Geophysical Research 93, 3232–3242.

Vasco, D.W., Smith, R.B., Taylor, C.L., 1990. Inversion for sources of crustal deformation and gravity change at the Yellowstone Caldera. Journal of Geophysical Research 95, 19839–19856.

Vasco, D.W., Karasaki, K., Myer, L., 1998. Monitoring of fluid injection and soil consolidation using surface tilt measurements. Journal of Geotechnical and Geoenvironmental Engineering 124, 29–37.

Vasco, D.W., Karasaki, K., Doughty, C., 2000. Using surface deformation to image reservoir dynamics. Geophysics 65, 132–147.

Vasco, D.W., Wicks, C. Jr., Karasaki, K., Marques, O., 2001a. Geodetic imaging: high resolution reservoir monitoring using satellite interferometry. Geophysical Journal International (in press).

Vasco, D.W., Karasaki, K. Kishida, K., 2001b. A coupled inversion of pressure and surface displacement. Water Resources Research (in press).

Ward, S.N., Barrientos, S.E., 1986. An inversion for slip distribution and fault shape from geodetic

observations of the 1983, Borah Peak, Idaho, earthquake. Journal of Geophysical Research 91, 4909–4919.

Wicks Jr., C., Thatcher, W., Dzurisin, D., 1998. Migration of fluids beneath Yellowstone caldera inferred from satellite radar interferometry. Science 282, 458–462.

Wright, C.A., Davis, E.J., Minner, W.A., Ward, J.F., Weijers, L., Schell, E.J., Hunter, S.P., 1998. Surface tiltmeter fracture mapping reaches new depths-10,000 feet and beyond? Society of Petroleum Engineering 39919, April.